

REVIEW

Open Access



# Heterogeneous catalysts for catalytic CO<sub>2</sub> conversion into value-added chemicals

Ho Seok Whang, Jinkyu Lim, Min Suk Choi, Jonghyeok Lee and Hyunjoo Lee\*

## Abstract

As climate change becomes increasingly evident, reducing greenhouse gases including CO<sub>2</sub> has received growing attention. Because CO<sub>2</sub> is thermodynamically very stable, its conversion into value-added chemicals such as CO, CH<sub>4</sub>, or C<sub>2</sub>H<sub>4</sub> is difficult, and developing efficient catalysts for CO<sub>2</sub> conversion is important work. CO<sub>2</sub> can be converted using the gas-phase reaction, liquid-phase reaction, photocatalytic reaction, or electrochemical reaction. The gas-phase reaction includes the dry reforming of methane using CO<sub>2</sub> and CH<sub>4</sub>, or CO<sub>2</sub> hydrogenation using CO<sub>2</sub> and H<sub>2</sub>. The liquid-phase reaction includes formic acid formation from pressurized CO<sub>2</sub> and H<sub>2</sub> in aqueous solution. The photocatalytic reaction is commonly known as artificial photo-synthesis, and produces chemicals from CO<sub>2</sub> and H<sub>2</sub>O under light irradiation. The electrochemical reaction can produce chemicals from CO<sub>2</sub> and H<sub>2</sub>O using electricity. In this review, the heterogeneous catalysts used for the gas-phase reaction or electrochemical reactions are discussed, because the liquid-phase reaction and photocatalytic reaction typically suffer from low productivity and poor durability. Because the gas-phase reaction requires a high reaction temperature of > 600 °C, obtaining good durability is important. The strategies for designing catalysts with good activity and durability will be introduced. Various materials have been tested for electrochemical conversion, and it has been shown that specific metals can produce specific products, such as Au or Ag for CO, Sn or Bi for formate, Cu for C<sub>2</sub>H<sub>4</sub>. Other unconventional catalysts for electrochemical CO<sub>2</sub> reduction are also introduced.

**Keywords:** Carbon dioxide, Dry reforming, Reverse water-shift reaction, Hydrogenation, Electrochemical reduction

## Background

Global energy consumption has soared due to increasing population and industrialization, and anthropogenic CO<sub>2</sub> emissions have rapidly grown because the main energy resources being consumed today are fossil fuels. Increasing CO<sub>2</sub> concentration in the atmosphere is leading to global warming and a range of environmental problems. Global average temperatures have increased by 0.8 °C over the last 70 years [1]. International efforts have been proposed to reduce CO<sub>2</sub> emissions, such as the multinational Paris agreement. At the same time, many studies have focused on the development and application of renewable energy sources as a means of reducing dependence on fossil fuels [2, 3], as well as technologies for capturing and utilizing CO<sub>2</sub>. CO<sub>2</sub> utilization would reduce greenhouse gases in the atmosphere and oceans

where they can do harm, and CO<sub>2</sub> can also be used to produce valuable chemicals [4–6].

Because CO<sub>2</sub> is thermodynamically the most stable carbon species, its conversion into value-added products usually requires the expenditure of considerable energy. Various chemical processes have been reported that can convert CO<sub>2</sub> into chemicals such as CO, hydrocarbon, or oxygenated hydrocarbon. Gas-phase reaction, liquid-phase reaction, electrochemical, and photocatalytic reaction methods have been reported. Gas-phase reactions include the dry reforming of methane (CH<sub>4</sub> + CO<sub>2</sub> → 2CO + 2H<sub>2</sub>), CO<sub>2</sub> hydrogenation (CO<sub>2</sub> + H<sub>2</sub> → CO + H<sub>2</sub>O, which is also called the reverse water-gas shift reaction; CO<sub>2</sub> + 4H<sub>2</sub> → CH<sub>4</sub> + 2H<sub>2</sub>O). The liquid-phase reaction includes the production of formic acid using CO<sub>2</sub> dissolved in aqueous phase (CO<sub>2</sub> (aq) + H<sub>2</sub> (aq) → COOH). Several review papers about CO<sub>2</sub> hydrogenation can be found in the literatures [7–9]. However, CO<sub>2</sub> hydrogenation or formic acid formation requires H<sub>2</sub>, which is mainly produced from

\* Correspondence: [azhyun@kaist.ac.kr](mailto:azhyun@kaist.ac.kr)

Department of Chemical and Biomolecular Engineering, Korea Advanced Institute of Science and Technology, Daejeon 34141, Republic of Korea



methane by steam reforming, which also produces a large amount of  $\text{CO}_2$ .

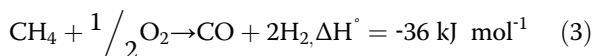
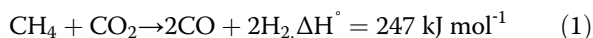
Electrochemical  $\text{CO}_2$  reduction has received a great deal of attention recently, but the low solubility of  $\text{CO}_2$  in aqueous solution has been a major obstacle. The use of a gas diffusion electrode has enabled the direct use of gaseous  $\text{CO}_2$  for electrochemical conversion. This electrochemical conversion process does not require  $\text{H}_2$  as a reactant. Photocatalytic  $\text{CO}_2$  conversion also received growing attention because of its similarity to photosynthesis, but the process typically suffers from low productivity and poor stability.

Efficient catalysts can minimize the energy needed for reactions by reducing the activation energy. Various catalysts are being actively investigated to enhance  $\text{CO}_2$  conversion and to control selectivity toward specific target products. In this review, we will focus on the heterogeneous catalysts for gas-phase  $\text{CO}_2$  conversion and electrochemical  $\text{CO}_2$  conversion. In the gas-phase  $\text{CO}_2$  conversion, catalysts used for the dry forming of methane,  $\text{CO}_2$  hydrogenation producing  $\text{CO}$ , and  $\text{CO}_2$  hydrogenation producing  $\text{CH}_4$  will be discussed. In the electrochemical  $\text{CO}_2$  conversion, the specific catalysts used to produce  $\text{CO}$ , formic acid, and hydrocarbons will be discussed. Reviews of formic acid formation or photocatalytic  $\text{CO}_2$  conversion can be found in the literature [10, 11].

## Catalytic $\text{CO}_2$ conversion in gas phase

### Dry reforming of methane

The dry reforming of methane (DRM) (Eq. (1)) can consume two greenhouse gases ( $\text{CO}_2$  and  $\text{CH}_4$ ) simultaneously and produce synthesis gas (abbreviated syn-gas, a mixture of  $\text{CO}$  and  $\text{H}_2$ ). The ratio of  $\text{H}_2$  to  $\text{CO}$  products is 1, which is much lower than other reforming reactions, such as the steam reforming of methane (SRM) and partial oxidation of methane (POM) (Eqs. (2) and (3)). The low ratio of  $\text{H}_2/\text{CO}$  is useful for synthesizing long chain hydrocarbons via the Fischer-Tropsch reaction [12–14].



The DRM reaction is endothermic, requiring a high reaction temperature of  $>700^\circ\text{C}$ , which results in high energy cost [15, 16]. Figure 1 shows the DRM equilibrium plots at various temperatures and 1 atm [17]. The high temperature is required to attain high product yield. Side reactions such as the reverse water gas shift

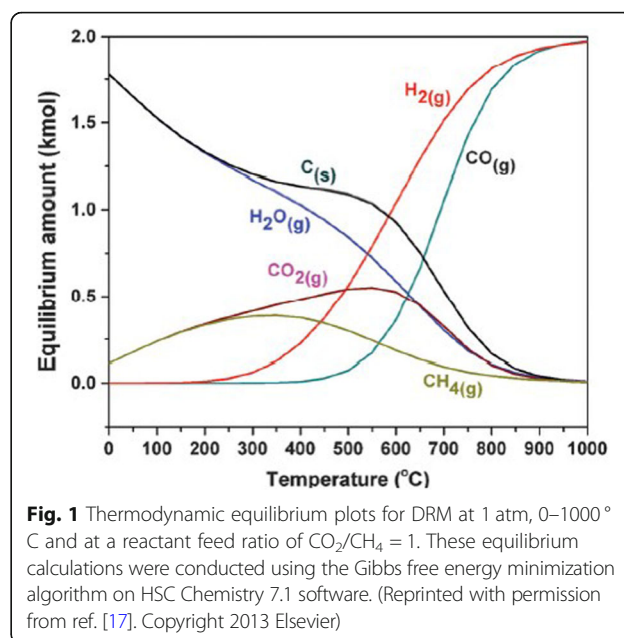
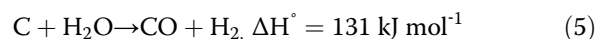
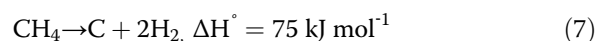
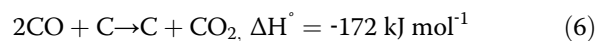


**Fig. 1** Thermodynamic equilibrium plots for DRM at 1 atm, 0–1000 °C and at a reactant feed ratio of  $\text{CO}_2/\text{CH}_4 = 1$ . These equilibrium calculations were conducted using the Gibbs free energy minimization algorithm on HSC Chemistry 7.1 software. (Reprinted with permission from ref. [17]. Copyright 2013 Elsevier)

(RWGS) reaction (Eq. (4)) or carbon gasification reaction (Eq. (5)) can occur. The RWGS reaction affects the  $\text{H}_2/\text{CO}$  ratio; because the RWGS reaction happens more, the  $\text{H}_2/\text{CO}$  ratio decreases and  $\text{CO}_2$  conversion increases. The steam produced from the RWGS reaction can react with carbon and produce syn-gas.



Also, deactivation occurs easily due to sintering and coke deposition, which degrades long-term durability [12, 18–20]. Carbon is produced due to the Boudouard reaction and methane cracking (Eq. (6) and Eq. (7)). The carbon is thermodynamically the main product at temperatures lower than  $570^\circ\text{C}$  [17]. DRM can proceed above  $640^\circ\text{C}$  with methane cracking. The Boudouard reaction can't occur above  $820^\circ\text{C}$ . Carbon can be produced by the Boudouard reaction, and methane cracking occurs from  $570$  to  $700^\circ\text{C}$  [21]. Coke deposition is thermodynamically favored at low temperature. The carbon produced by methane cracking is likely to react with steam or carbon dioxide at high temperature. Thus, the DRM reaction should be performed at high temperature.



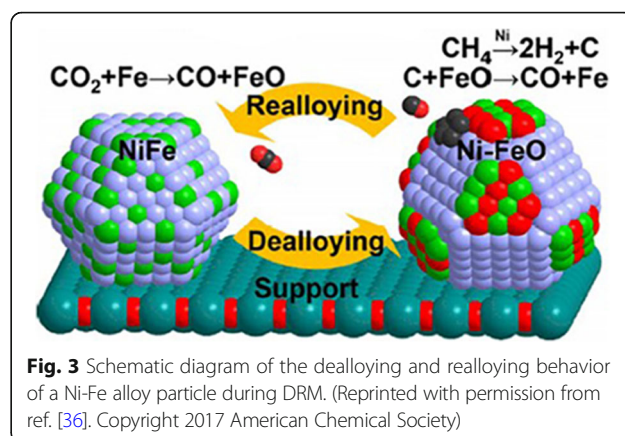
Various heterogeneous catalysts have been developed, including metal supported catalysts, perovskites, and solid solution catalysts [22–26]. Precious metals (Pt, Rh

or Ru) are known to have high activity and durability, although at high price. Non-precious metals (Ni or Co) have been widely investigated as well. In this section, each component of DRM catalysts will be explained, and the strategies to enhance their activity and durability for DRM will be demonstrated.

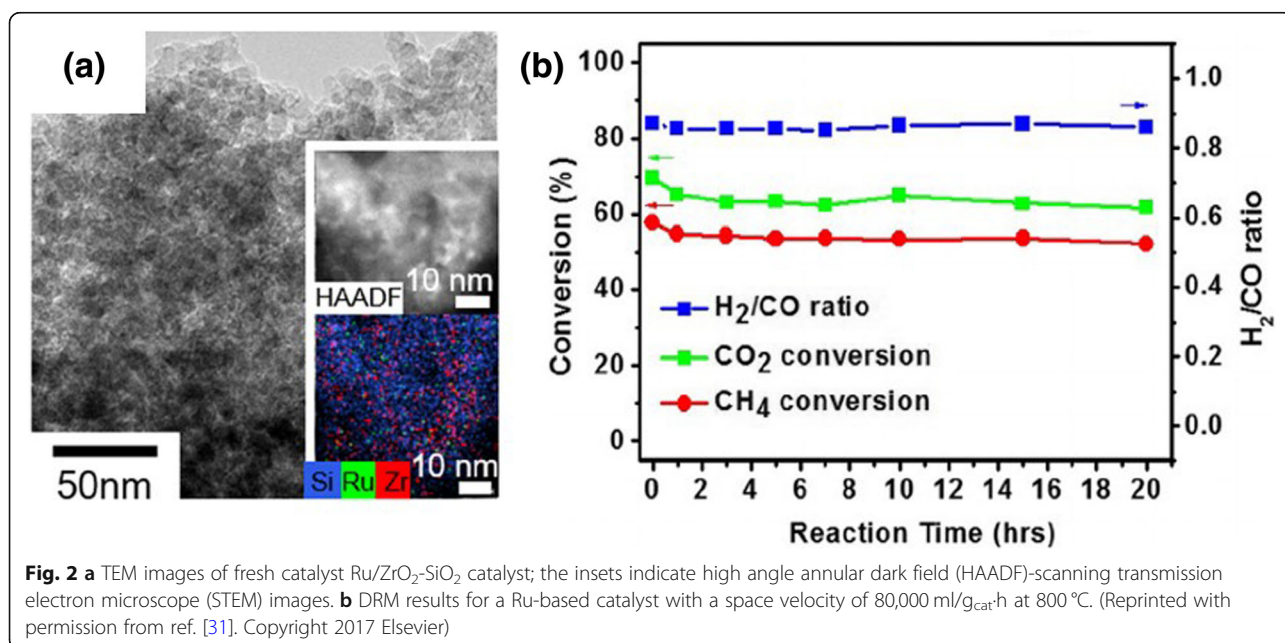
#### Compositions of the catalysts: Metal, supports, promoters

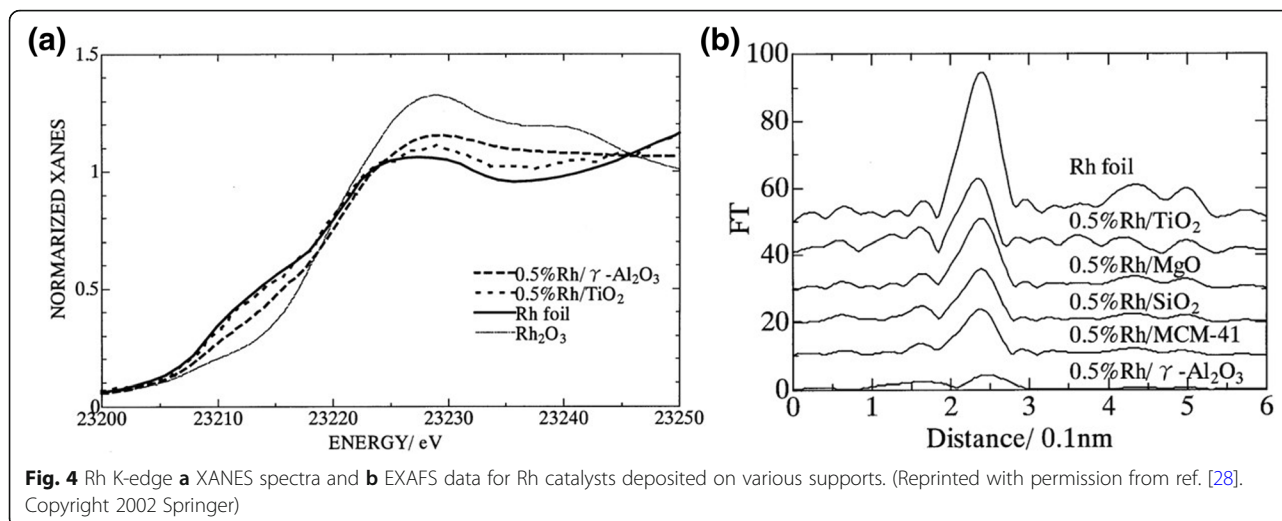
Precious metals such as Pt, Rh and Ru are highly active for DRM and also resistant against coke deposition [27–30]. The precious metal-based catalysts show high activity in spite of the very small amount of metal catalyst used. For example, the Ru/ZrO<sub>2</sub>-SiO<sub>2</sub> catalyst shows high activity and durability, as shown in Fig. 2, even though the Ru content was only 0.13 wt% [31].

Non-precious metals such as Ni or Co have been used more for DRM due to their cheap price and abundance [32–34]. Ni catalysts have shown a level of activity comparable to precious metals [30]. Alloyed metal catalysts are widely used for DRM because they have a different electronic structure than monometallic materials [35]. For example, the Ni-Fe alloy catalyst exhibited interesting behavior for DRM, as shown in Fig. 3. Monometallic Ni or Fe catalysts have shown poor durability, because the monometallic Ni catalyst is easily deactivated by coke deposition, and Fe is inactive for DRM. During the DRM reaction, the Ni-Fe alloy surface is partially oxidized; Ni maintains an oxidation state, while Fe is oxidized by CO<sub>2</sub>. The oxidized FeO causes dealloying of the surface, and the FeO then oxidizes the carbon deposited on the surface, returning to Fe. The Fe<sup>2+</sup>/Fe redox cycle plays a key role in enhancing durability in the DRM reaction [36].



Supports can affect catalytic activity and durability for DRM [37]. The interaction between a support and metal can change the dispersion of the metal, resistance against sintering, and the electronic structure of the metal [28, 31]. Figure 4 shows the X-ray absorption fine structure (XAFS) analysis results of Rh catalysts deposited on various supports of Al<sub>2</sub>O<sub>3</sub>, TiO<sub>2</sub>, etc. The X-ray absorption near edge structure (XANES) analysis in Fig. 4a shows that the Rh electronic structure has changed as a result of the support materials. TiO<sub>2</sub> supported Rh has a metallic character, while γ-Al<sub>2</sub>O<sub>3</sub> supported Rh has an oxidic character. Figure 4b shows extended X-ray absorption fine structure (EXAFS) spectra. The Rh-Rh peak at 0.24 nm has different intensities with various supports. When the intensity is higher, the Rh-Rh coordination number is higher, indicating lower dispersion. The support materials affect the dispersion of the metal and chemical environment. [28].





The strong-metal support interaction (SMSI) causes a high dispersion of metals resulting in small sized metal nanoparticles with enhanced DRM activity. In addition, it increases resistance against sintering with enhanced durability [31, 38, 39]. The acidity and basicity of the support also affects catalytic properties. CO<sub>2</sub> is activated by forming formate with surface hydroxyl on an acidic support. CO<sub>2</sub> is activated by forming oxy-carbonate on a basic support. On an inert support such as SiO<sub>2</sub>, both CO<sub>2</sub> and CH<sub>4</sub> are activated by metal with faster deactivation. A DRM catalyst supported on an inert material (SiO<sub>2</sub>) is usually less active and less durable than on an acidic support (Al<sub>2</sub>O<sub>3</sub>) or basic support (La<sub>2</sub>O<sub>3</sub>) [23, 30, 40, 41].

Promoters have been widely used for DRM. Alkali metal oxides such as K<sub>2</sub>O or CaO have been used to increase the basicity of the catalyst enhancing CO<sub>2</sub> adsorption [42–44]. CeO<sub>2</sub> or ZrO<sub>2</sub> were used to increase oxygen mobility [22, 45–50]. The transition between Ce<sup>3+</sup> and Ce<sup>4+</sup> can occur easily on CeO<sub>2</sub>. The coke formed on Ni sites could be oxidized by using the redox cycle of CeO<sub>2</sub> with enhanced coke-resistivity [47]. The surface hydroxyl group can participate in the DRM surface reaction. Zhu et al. reported that the energy barrier for CH and C oxidation by surface OH was slightly lower than the barrier for surface O [51]. Ni et al. showed that the surface hydroxyl groups were increased by adding B<sub>2</sub>O<sub>3</sub> to Ni catalyst, as shown in Fig. 5. The surface hydroxyl groups oxidize the carbon formed from methane decomposition, with enhanced resistance against coke deposition [52].

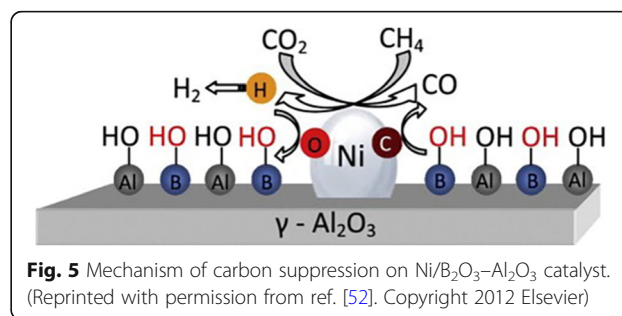
#### Coke-resistant catalysts

The key objective of catalysts developed for DRM is how to prevent coke deposition. Highly durable catalysts should avoid sintering because large Ni particles have severe coke formation at the surface, while small Ni

nanoparticles do not have carbon deposition. In this section, various strategies to control the nano-structures of catalysts to prevent coke deposition will be discussed.

In order to prevent the sintering of nanoparticles, an inorganic oxide overlayer was formed on Ni nanoparticles [53–57]. As shown in Fig. 6, Ni nanoparticles with an average size of 5 nm were immobilized on SiO<sub>2</sub> spheres, then porous SiO<sub>2</sub> overlayers were formed on the Ni nanoparticles. The resulting Ni/SiO<sub>2</sub>@SiO<sub>2</sub> catalyst showed high durability for DRM; activity was maintained for 170 h at 800 °C without Ni sintering [53].

Using this nano-structure, the effects of Ni size and support were evaluated independently. To evaluate the size effect, various sizes of Ni nanoparticles were deposited; 2.6, 5.2, 9.0, 17.3 nm. CH<sub>4</sub> turnover frequency clearly increased as Ni size decreased. The size effect could be evaluated exactly because the Ni size was barely changed even after the DRM reaction at 800 °C. The different metal oxide overlayers of Al<sub>2</sub>O<sub>3</sub>, MgO, ZrO<sub>2</sub>, TiO<sub>2</sub>, SiO<sub>2</sub> were formed on Ni/SiO<sub>2</sub> with a Ni particle size of 5.2 nm. The Al<sub>2</sub>O<sub>3</sub> and MgO overlayers showed enhanced CH<sub>4</sub> turnover frequency, while the other overlayers hardly showed enhancement [55].



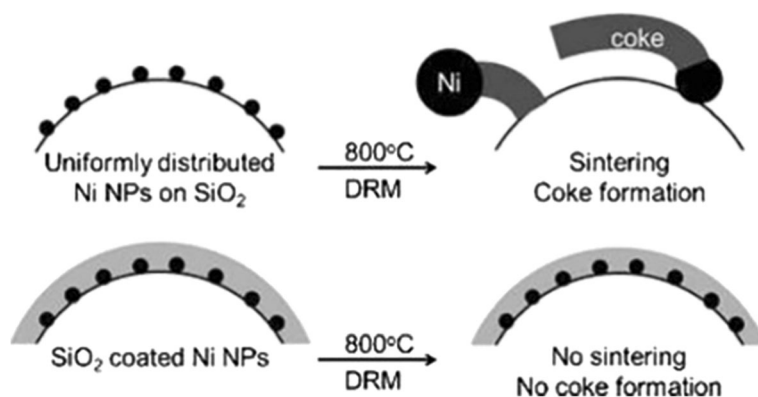


**Fig. 6** Schematic illustration of Ni/SiO<sub>2</sub>@SiO<sub>2</sub> catalyst with high coke resistance for the DRM reaction. (Reprinted with permission from ref. [53]. Copyright 2014 John Wiley and Sons)

Similarly, core-shell structures have been investigated; an outer shell such as SiO<sub>2</sub> separates the catalytic core material such as Ni nanoparticles while preventing sintering [58, 59]. The core-shell structures have been widely used in DRM, CO oxidation, and methane combustion reactions [60–62]. Li et al. developed a Ni yolk@Ni@SiO<sub>2</sub> catalyst, where a SiO<sub>2</sub> shell with Ni nanoparticles embedded in the middle surrounds a Ni yolk core. This catalyst was highly active for DRM, and it maintained activity without sintering for 90 h at 800 °C [62].

Mesoporous materials have been widely used as supports because they provide a large surface area and facile mass transfer [63, 64]. Mesoporous Al<sub>2</sub>O<sub>3</sub> in particular has been widely used because it can have a strong interaction with a metal active phase, and it has high thermal stability [65, 66]. Conventional impregnation with a metal precursor might cause pore blockage. Wang et al. developed ordered mesoporous Ni-Ce-Al oxide for DRM with self-assembly induced by solvent evaporation [67]. The Ni nanoparticles were uniformly deposited in the pore channel of the mesoporous support. The catalysts showed high durability because the Ni nanoparticles did not sinter severely due to spatial confinement. It maintained high DRM activity for 80 h at 700 °C.

### CO<sub>2</sub> hydrogenation

#### Reverse water-gas shift reaction

CO<sub>2</sub> can react with H<sub>2</sub> to produce CO via the reverse water gas shift reaction. The RWGS reaction was first observed in 1914 by Bosch and Wild when they tried to produce H<sub>2</sub> from steam and CO over FeO<sub>x</sub> catalyst [68]. RWGS can produce syn-gas, which is useful for synthesizing valuable chemicals such as ammonia, methanol, and fuels, from CO<sub>2</sub> [69]. However, the RWGS reaction is endothermic, requiring high temperature, and CO is the dominant product above 600 °C as can be seen in

Fig. 7 [70]. Developing catalysts with high activity and durability is essential to obtain a maximum yield.

Two reaction pathways, the redox mechanism and formate decomposition mechanism, have been reported for CO formation from RWGS. A case with a Cu catalyst followed the redox mechanism; CO<sub>2</sub> oxidizes Cu<sup>0</sup> to Cu<sup>+</sup> generating CO, and H<sub>2</sub> reduces Cu<sup>+</sup> to Cu<sup>0</sup> forming H<sub>2</sub>O [71]. In the formate decomposition mechanism, CO<sub>2</sub> hydrogenates to formate, followed by cleavage of the C=O bond [72]. Catalysts for RWGS should contain active sites to dissociate hydrogen and adsorb CO<sub>2</sub>. Precious metal-based catalysts have been widely used for RWGS because of their superior activity for hydrogen dissociation. The effect of Pt particle size on the

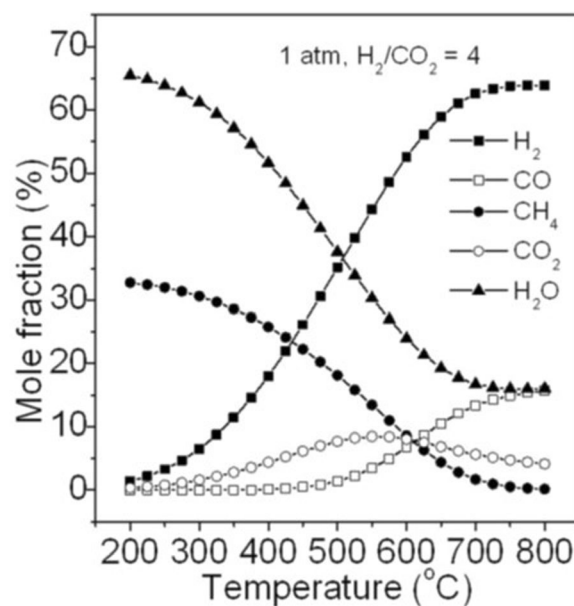


**Fig. 7** Thermodynamic equilibrium of CO<sub>2</sub> hydrogenation at 1 bar and a H<sub>2</sub>/CO<sub>2</sub> molar ratio of 4. (Reprinted with permission from [70]. Copyright 2012 Royal Society of Chemistry)

selectivity of CO and CH<sub>4</sub> was identified using rutile TiO<sub>2</sub> as a support. Small Pt particles preferred CO formation. Pt-CO species were the key intermediate deciding CO selectivity in the RWGS reaction [73].

The Au@UIO-67 catalyst was synthesized for the RWGS reaction. UIO-67, which is porous metal-organic framework, was used to disperse Au nanoparticles, then the interaction between the metal and support was enhanced. Au@UIO-67 showed high activity and CO selectivity for RWGS [74]. A Pd-In/SiO<sub>2</sub> catalyst was synthesized by the wet impregnation method and used for RWGS. While the Pd/SiO<sub>2</sub> showed 88% CO selectivity, Pd-In/SiO<sub>2</sub> showed 100% CO selectivity without CH<sub>4</sub> formation. The difference was derived from the modified CO adsorption energy. CO adsorption on the Pd-In bimetallic surface was much weaker than that on the Pd surface [75].

For the large scale conversion of CO<sub>2</sub>, non-precious metal catalysts are preferred due to cost and scarcity. Ni and Cu-based catalysts are promising because they also show high activity and selectivity for RWGS. But they usually suffer from sintering at high reaction temperatures.

Various ways of improving thermal stability have been investigated. Rossi et al. prepared highly dispersed Ni nanoparticles supported on SiO<sub>2</sub> using magnetron sputtering deposition. The prepared catalyst showed better activity at T > 600 °C and stability than a conventional catalyst prepared by the wet impregnation method [76]. Ni/Ce-Zr-O catalysts were synthesized and used for RWGS. Ni species were incorporated into the lattice of a Ce-Zr-O solid solution. High activity, stability and selectivity were achieved for the conversion of CO<sub>2</sub> to CO [77]. Cu/ZnO catalysts with various Cu/Zn ratios were synthesized using aurichalcite precursors. The interface between the Cu and ZnO affected the catalytic activity for CO<sub>2</sub> activation. As the Cu ratio increased, the Cu domain size increased and the CO generation rate decreased [78]. Zheng et al. prepared CeCu composite catalysts with different Ce/Cu mole ratios for RWGS. The Ce<sup>3+</sup>-oxygen vacancy-Cu<sup>0</sup> structure was stabilized. Cu sites became more electron deficient following electron transfer from Cu to Ce, with enhanced adsorption of CO<sub>2</sub> and H<sub>2</sub>. The Ce<sub>1.1</sub>Cu<sub>1</sub> catalyst showed the highest catalytic performance for the RWGS reaction [79].

Transition-metal carbides (TMCs) are promising for RWGS because they can dissociate hydrogen and C=O bonds. With their abundance and low cost, many researchers have reported on TMCs based-catalysts for RWGS. A recent study revealed that Mo<sub>2</sub>C showed higher CO<sub>2</sub> conversion and CO selectivity in the RWGS than other TMCs such as TiC, TaC, ZrC, WC, and NbC [80]. The experimental and density functional theory (DFT) results showed that the oxygen binding energy

and activation barriers for oxygen removal were the main factors for identifying effective catalysts for CO<sub>2</sub> reduction.

Willauer et al. prepared K-Mo<sub>2</sub>C supported on γ-Al<sub>2</sub>O<sub>3</sub> [81]. By modifying with a K promoter, CO selectivity and stability increased, with only 7.3% deactivation after 68 h. CO<sub>2</sub> adsorption was enhanced and CO<sub>2</sub> dissociation barriers were reduced on the K-promoted catalyst. Illas et al. reported that polycrystalline α-Mo<sub>2</sub>C catalyst showed 16% CO<sub>2</sub> conversion and 99.5% CO selectivity at 673 K in RWGS [82]. The presence of a (101)-Mo/C surface on the catalyst provides active sites for RWGS. Ma et al. synthesized a highly efficient and stable Cu/β-Mo<sub>2</sub>C catalyst for the RWGS reaction [83]. Because of strong interaction between the Cu and β-Mo<sub>2</sub>C which dispersed the Cu particles uniformly on the support, Cu/β-Mo<sub>2</sub>C showed high activity and stability compared with Pt- and Cu-based catalysts. Recently, Ajayan et al. reported a metal-free carbon-based catalyst for CO<sub>2</sub> hydrogenation [84]. Pyridinic N was doped at the edge sites of graphene quantum dots. The N dopants played a key role in inducing thermocatalytic CO<sub>2</sub> hydrogenation activity. CO was produced dominantly at lower temperatures and CO selectivity increased to 85% at 300 °C.

Recently, Ajayan et al. reported a metal-free carbon-based catalyst for CO<sub>2</sub> hydrogenation [84]. Pyridinic N was doped at the edge sites of graphene quantum dots. The N dopants played a key role in inducing thermocatalytic CO<sub>2</sub> hydrogenation activity. CO was produced dominantly at lower temperatures and CO selectivity increased to 85% at 300 °C.

### CO<sub>2</sub> methanation

CO<sub>2</sub> hydrogenation can also produce methane. The CO<sub>2</sub> methanation has recently received much attention as a way to store intermittent electricity, which is produced from solar cell or wind power [85]. The surplus electricity can electrolyze water, producing H<sub>2</sub>. Then CO<sub>2</sub> and the H<sub>2</sub> can have reaction to produce methane, which can be used as a fuel. Various precious metals, such as Ru, Rh, Pd, have been used as catalyst. Ni deposited on various supports have also been used for the CO<sub>2</sub> methanation [85]. Amal and Dai et al. produced methane from CO<sub>2</sub> and H<sub>2</sub> using porous perovskite materials [86, 87]. The perovskite materials with ABO<sub>x</sub> crystalline structure have been particularly interesting materials in solar cells or catalytic applications [86]. Ni-Rh nanoalloy nanoparticles were formed by ex-solution on mesoporous LaAlO<sub>3</sub> perovskite and showed good performance for CO<sub>2</sub> methanation with turnover frequency of 13.9 mol/mol/h [87]. Similarly, mesoporous Ni/Co<sub>3</sub>O<sub>4</sub> was

prepared with high activity for CO<sub>2</sub> methanation at low temperature [88].

### Light-assisted CO<sub>2</sub> hydrogenation

Light is considered an important and ultimate energy source for CO<sub>2</sub> reduction, in a process also known as artificial photosynthesis. Various semiconductor-based photocatalysts have been investigated for CO<sub>2</sub> reduction [89, 90]. However, they typically have shown low activity and poor durability. Instead of using light for exciton production, light can be used as an auxiliary energy source to minimize overall energy usage. Recently, unique light-assisted surface reactions have been reported [91–93]. They can occur through excitation of electrons in hybridized orbitals of adsorbed reactant molecules on the metal catalyst surface.

We recently reported light-assisted CO<sub>2</sub> hydrogenation on heterogeneous metal catalysts [94]. Various metals were tested in a photoreactor by changing temperature, light intensity, and light wavelength. CO<sub>2</sub> conversion was enhanced on a Ru or Rh catalyst upon light irradiation, as shown in Fig. 8a. They produced CH<sub>4</sub> selectively. But Pt, Ni, Cu only produced CO without any enhancement upon light irradiation. As the light

intensity increased, CO<sub>2</sub> conversion also increased linearly, indicating that hot electrons generated upon light irradiation were responsible for the CO<sub>2</sub> conversion enhancement.

In-situ UV spectroscopy results measured under CO<sub>2</sub> flow also confirmed that CO<sub>2</sub> adsorbed on the Ru surface can absorb visible light. DFT calculations showed that the band-gap energy decreased from 8.2 eV for free CO<sub>2</sub> to 2.4 eV for CO<sub>2</sub> adsorbed on Ru, as shown in Fig. 8b. This small band-gap energy enabled the absorption of visible light. The DRIFT measurement in Fig. 8c shows that CO<sub>2</sub> was cleaved to CO with light irradiation on a Ru catalyst. By using both light and heat, the overall energy could be reduced to 37% of the case when only heat was used, to achieve the same CO<sub>2</sub> conversion of 15%. Additionally, the CO<sub>2</sub> conversion was easily initiated or terminated simply by turning the light on or off.

### Electrochemical CO<sub>2</sub> reduction

The electrochemical CO<sub>2</sub> reduction reaction (CO<sub>2</sub>RR) involves CO<sub>2</sub> conversion on an electrode powered by electric bias. Because CO<sub>2</sub> is highly stable with a linear molecular shape having two C=O bonds, it requires a high overpotential to initiate the reaction [95]. An overpotential is the difference between the actual applied

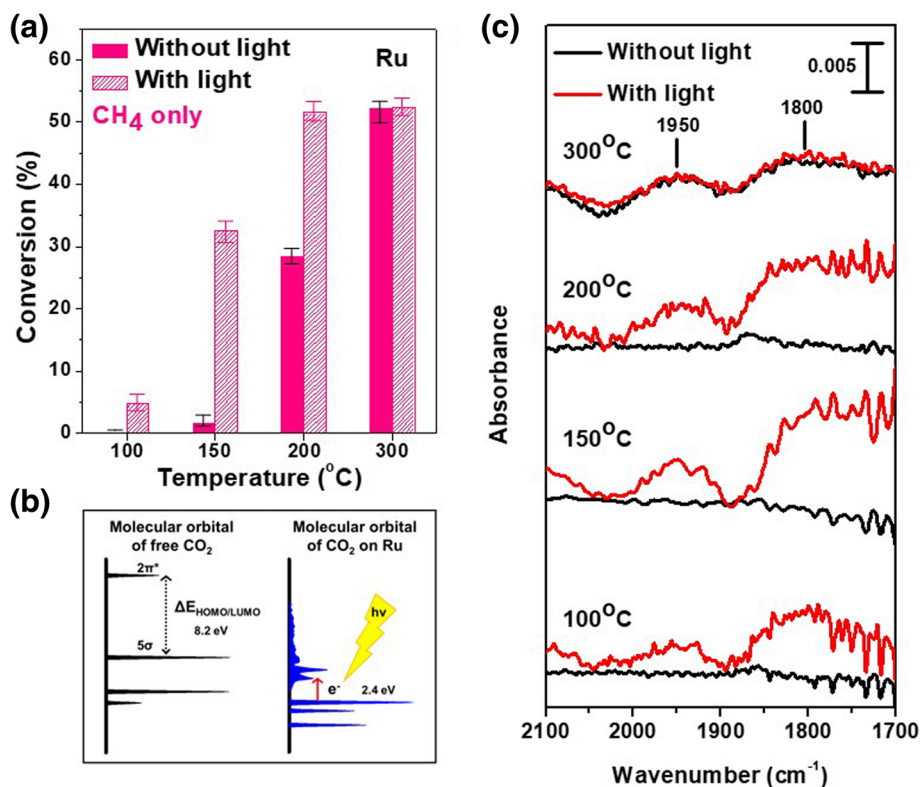


**Fig. 8** a CO<sub>2</sub> conversion enhancement with light irradiation at various temperatures, b schematic diagram of hybridized orbital change and hot electron generation with light irradiation, c DRIFT analysis results with CO<sub>2</sub> flow on Ru catalysts with and without light irradiation. (Reprinted with permission from ref. [94]. Copyright 2018 Springer Nature)

potential and theoretical thermodynamic potential. Heterogeneous electrocatalysts should be used to reduce the overpotential. The performance and reaction pathway highly depend on the electrocatalyst. CO<sub>2</sub> is electrochemically reduced to chemicals or fuels at the cathode, and the counter anode reaction is water oxidation producing oxygen, typically known as oxygen evolution reaction (OER) [96].

A distinct feature of the electrochemical CO<sub>2</sub> reduction is its compatibility with renewable sources. Because CO<sub>2</sub> is thermodynamically stable, the CO<sub>2</sub> conversion involves high energy consumption [95, 97]. This energy can be obtained from renewable sources, such as solar or wind power, and the obtained electricity can drive the electrochemical CO<sub>2</sub>RR. Additionally, electrochemical CO<sub>2</sub> conversion can be used for renewable energy storage [95, 98]. Since the renewable power is inherently intermittent and undistributed, storing the electricity in chemical bonds might be useful [98]. Fuels such as CH<sub>4</sub> can be used in current conventional power systems. Various chemicals, from several C<sub>1</sub> products to multi-carbon products, can be directly generated from electrochemical CO<sub>2</sub>RR [99–101].

Various products can be obtained from the electrochemical CO<sub>2</sub>RR. Table 1 shows several representative CO<sub>2</sub>RR pathways with thermodynamic standard potentials versus a reversible hydrogen electrode (RHE) [96, 102]. Neutral pH buffer electrolytes have been widely used for electrochemical CO<sub>2</sub>RR studies, and the potentials at neutral pH were shown [96]. The CO<sub>2</sub>RR typically competes with the hydrogen evolution reaction (HER). Suppressing HER is one of the most important issues in the development of electrocatalysts for CO<sub>2</sub>RR. In this next section, the electrocatalysts are classified according to products of CO, formate, and multi-carbon species. The metals generating each product are explained. Unconventional catalysts are additionally introduced.

### Metals producing CO: Au, Ag, Zn, and Pd

Au, Ag, Zn, and Pd generate CO as a predominant product from CO<sub>2</sub>RR [101]. CO is an important feed chemical for various chemical processes [95]. The key descriptor for CO production is the binding energy of \*COOH. The metals bind to \*COOH sequentially yielding \*CO after dehydration, as shown in Fig. 9 [100, 103, 104]. The reaction pathway toward CO is two electron-consuming, which is relatively facile [100]. When CO is the main product, there is no separation issue because gaseous CO would be naturally separated from liquid electrolyte.

Various works controlling the nano-structures of these metals have been reported to have high CO production from CO<sub>2</sub>RR; monodispersed Au or Ag nanoparticles [105–108], ligand-free Au nanoparticles with < 2 nm [109], inverse opal Au or Ag thin films [110, 111], ultra-thin Au nanowires [112], Au nanoneedles with sharp tips [113, 114], concave rhombic dodecahedral Au nanoparticles with high-index facets [115], TiC-supported Au nanoparticles [116], hexagonal Zn particles [117], electrodeposited Zn dendrites [118], anodized Zn foil [119], small sized Pd nanoparticles with rich edge sites [120, 121], Au electrode with adsorbed CN<sup>-</sup> or Cl<sup>-</sup> ions [122], Ag nanoparticles with surface-bonded oxygen [123], amine-capped Ag nanoparticles [124]. Although it is hard to compare their performance because of their different reaction conditions, the conversion of CO<sub>2</sub> to CO usually reaches 90 ~ 100% faraday efficiency at the relatively low overpotential of 0.4 ~ 0.7 V.

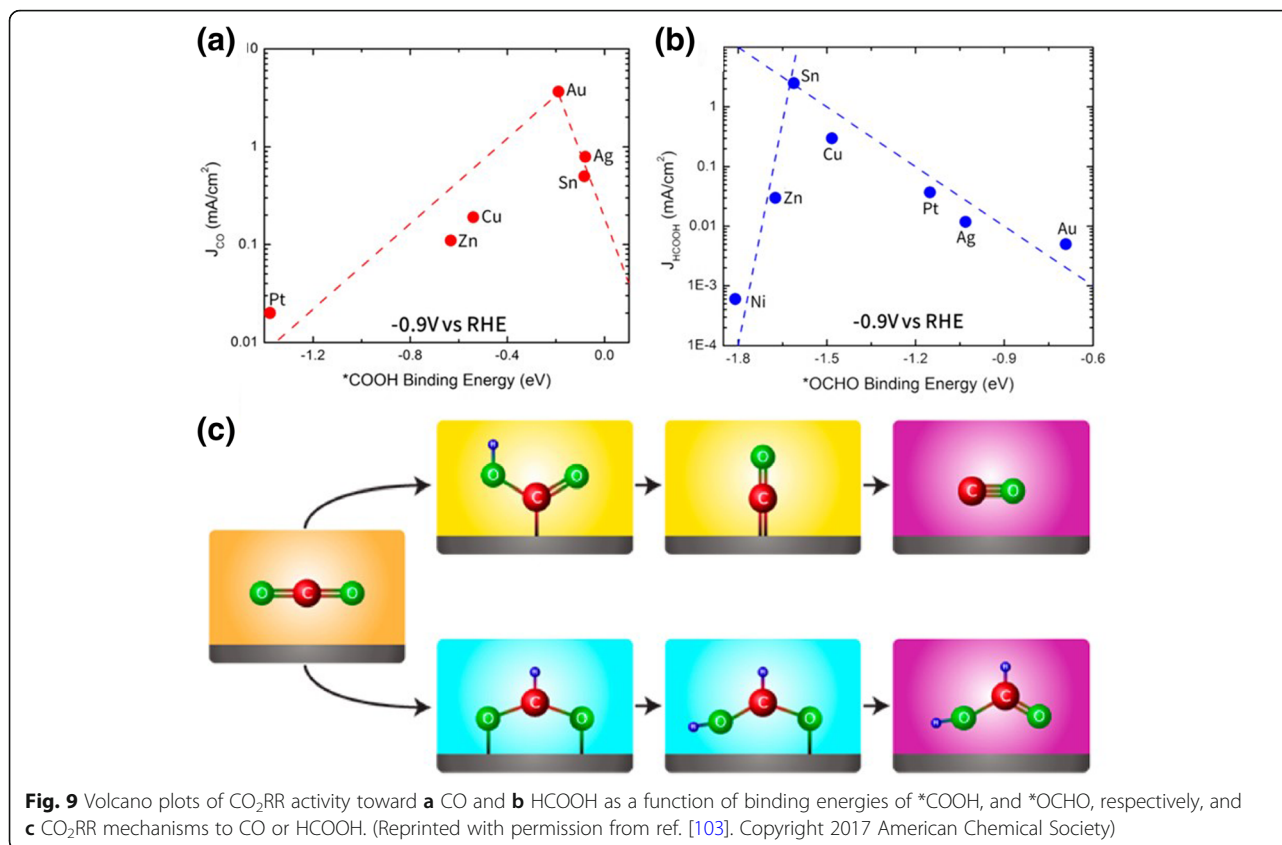
### Metals producing formate: Sn, Bi, Hg, Cd, and Pb

Sn, Bi, Hg, Cd, and Pb can produce formic acid (HCOOH) or formate (HCOO<sup>-</sup>) in the CO<sub>2</sub>RR [101]. The key descriptor toward formate formation is the binding energy of \*OCHO [103]. If the electrode surface is bound to intermediates via oxygen rather than carbon, formic acid will be generated, as shown in Fig. 13 [103]. It was also suggested that formate could be generated through an \*COOH intermediate at some reaction

**Table 1** Representative reaction pathways of CO<sub>2</sub>RR in neutral pH buffer electrolyte condition with thermodynamic standard potentials

	Reaction in neutral pH buffer electrolyte	E <sup>0</sup> (V vs RHE)
Cathode reaction	(CO <sub>2</sub> RR) CO <sub>2</sub> + H <sub>2</sub> O + 2e <sup>-</sup> → CO + 2OH <sup>-</sup>	-0.10
	(CO <sub>2</sub> RR) CO <sub>2</sub> + 2H <sub>2</sub> O + 2e <sup>-</sup> → HCOOH + 2OH <sup>-</sup>	-0.02
	(CO <sub>2</sub> RR) CO <sub>2</sub> + 5H <sub>2</sub> O + 6e <sup>-</sup> → CH <sub>3</sub> OH + 6OH <sup>-</sup>	0.03
	(CO <sub>2</sub> RR) CO <sub>2</sub> + 6H <sub>2</sub> O + 8e <sup>-</sup> → CH <sub>4</sub> + 8OH <sup>-</sup>	0.17
	(CO <sub>2</sub> RR) 2CO <sub>2</sub> + 8H <sub>2</sub> O + 12e <sup>-</sup> → C <sub>2</sub> H <sub>4</sub> + 12OH <sup>-</sup>	0.08
	(HER) 2H <sub>2</sub> O + 2e <sup>-</sup> → H <sub>2</sub> + 2OH <sup>-</sup>	0
Anode reaction	(OER) 2H <sub>2</sub> O → O <sub>2</sub> + 4H <sup>+</sup> + 4e <sup>-</sup>	1.229





conditions [125, 126]. Because the pathway generating formates follows a two electron pathway, like CO, some electrocatalysts might exhibit good CO<sub>2</sub>RR performance for formic acid production [101]. However, the faradaic efficiency for formic acid production is usually lower than that for CO production [127]. Nevertheless, formic acid is the only liquid product which can be obtained with high selectivity from CO<sub>2</sub>RR at this stage [101].

Various studies which have controlled the nanostructures of these metals have been reported for formate production; nanostructured Sn/SnO<sub>x</sub> thin film [128], Sn or Sn oxide nanoparticles with < 5 nm [129, 130], reduced SnO<sub>2</sub> porous nanowires [131], hierarchical mesoporous SnO<sub>2</sub> nanosheets [132], electrodeposited Sn dendrites [133], atomic layer deposited Sn or Sn sulfide on nanoneedle templates [134], ultrathin Bi nanosheets [135], oxide-derived Pb [136]. Due to toxicity of Hg, Cd, and Pb, most works have mainly used Sn or Bi. The formate can be obtained with a faraday efficiency of 60 ~ 90% at an overpotential of 0.8 ~ 1.4 V [95, 101].

On other metals, the selectivity of CO<sub>2</sub>RR can be controlled by changing the reaction conditions to produce formic acid. For example, CO<sub>2</sub>RR on W, Fe, Co, Ni, Zn, Pt, Rh, and Ir have been investigated at high pressure [137]. They showed significant activity toward formate formation, although their selectivity was not as high as

Sn or Bi. Pd also exhibited good performance for formic acid production although it also significantly produced CO [138, 139].

#### Metal producing multi-carbon species: Cu

Cu is the only element that can make a C-C bond directly from CO<sub>2</sub>RR with meaningful selectivity [95, 101]. Multi-carbon products such as C<sub>2</sub>H<sub>4</sub> can be generated with Cu. Figure 10 shows the possible products obtainable from electrochemical conversion on a Cu electrode. It was reported that CO, formate, CH<sub>4</sub>, C<sub>2</sub>H<sub>4</sub>, and H<sub>2</sub> could be obtained on a Cu electrode [140]. Ethanol, n-propanol, allyl alcohol, a trace amount of methanol, glycolaldehyde, acetaldehyde, acetate, ethylene glycol, propionaldehyde, acetone, and hydroxyacetone were simultaneously observed in the large overpotential region, higher than 1 V [140].

The reaction mechanism of CO<sub>2</sub>RR on a Cu electrode is highly complicated. Figure 10 provides the possible reaction pathway maps. Many other pathways on the Cu electrode have also been proposed [141–143]. The \*CO intermediate is generally regarded to be a key intermediate for further reduction, because \*CO can be obtained at mild potentials, and C<sub>2</sub>H<sub>4</sub> was observed only with significant concentrations of \*CO [144–146]. The protonation of \*CO to \*CHO needs to overcome an activation

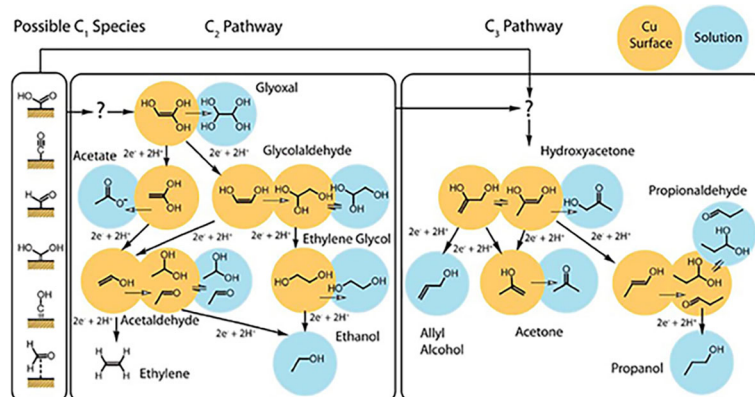


**Fig. 10** Proposed reaction pathways of electrochemical  $\text{CO}_2\text{RR}$  on Cu electrode in  $\text{CO}_2$ -saturated 0.1 M  $\text{KHCO}_3(\text{aq})$ . (Reprinted with permission from ref. [140]. Copyright 2012 Royal Society of Chemistry)

barrier of 0.74 V, which is considered a rate-determining step for further reduction to  $\text{C}_1$  products like  $\text{CH}_3\text{OH}$  or  $\text{CH}_4$  [145, 147]. The  $^*\text{CHO}$  transforms to  $^*\text{CH}_2\text{O}$ ,  $^*\text{CH}_3\text{O}$ , and  $^*\text{CH}_4$  following sequential proton coupled electron transfer (PCET) [142, 147]. The  $^*\text{CHO}$  is also a key intermediate for making C-C bonds via  $^*\text{CO}$ - $^*\text{CHO}$  coupling [143].

Additionally,  $^*\text{CO}$ - $^*\text{CO}$  coupling can also produce C-C bonds [141, 148–150]. However, the C-C coupling pathway has not been elucidated yet, although it is known that Cu (100) is the best surface to generate  $^*\text{CO}$ - $^*\text{CO}$  coupling with the lowest energy barrier [150, 151]. As a result,  $\text{C}_2\text{H}_4$  formation is favored on Cu (100) [151–153], whereas  $\text{CH}_4$  is more readily produced on Cu (111) [147, 154]. The pathways for further reduction from  $^*\text{CO}$ - $^*\text{CO}$  or  $^*\text{CHO}$ - $^*\text{CO}$  to oxygenates, such as acetate, ethanol, 1-propanol, are more complicated, because water from the electrolyte participates in the reaction donating oxygen [143, 148]. Because it is crucial to understand the reaction mechanism to design better catalysts for  $\text{CO}_2\text{RR}$ , more studies on mechanism or intermediates, such as in-situ experiments, are needed.

To tune selectivity, nano-structured Cu electrodes were studied, including Cu nanofoams [155], Cu nanowires [156–160], nanoporous Cu film [161], Cu nanocubes [151–153], Cu truncated nanocubes [153], Cu rhombic dodecahedrons [153], inverse opal Cu film [162], mesoporous Cu film [163], electro-redeposited Cu [164], electrodeposited Cu dendrites [165], prism shaped Cu [166], nano-structured Cu by battery cycling [150], hierarchical Cu pillar electrode [167], oxide derived Cu [160, 168–170]. The best  $\text{CO}_2\text{RR}$  performance on Cu electrode was 60 ~ 70% faraday efficiency toward  $\text{C}_2\text{H}_4$  production [170, 171].

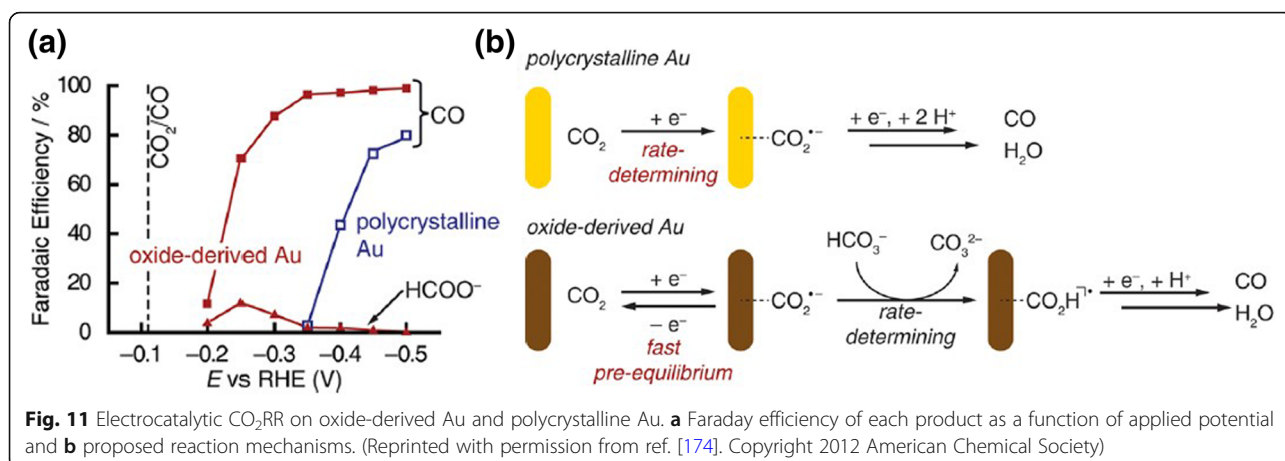
### Unconventional electrocatalysts

So far, electrochemical  $\text{CO}_2\text{RR}$  with single metal electrodes has been discussed. The studies with single metal electrodes can provide insight in terms of reaction mechanisms and the properties of each metal on  $\text{CO}_2\text{RR}$ . Some unconventional electrocatalysts, such as oxide-derived metals, alloy metals, carbon materials, single-atom catalyst, have also exhibited interesting features. Distinct selectivity or activity was obtained.

#### Oxide-derived metals

Recent studies have revealed that oxide-derived metal electrodes had improved catalytic performance compared to pristine metals [172]. The most common way to prepare oxide-derived electrocatalysts is to oxidize the metal, then reduce it to its original metallic state. Oxide-derived Cu produced more  $\text{C}_2$  products of  $\text{C}_2\text{H}_4$ ,  $\text{C}_2\text{H}_6$ , and ethanol than electro-polished Cu at the same overpotential [168, 170, 172]. Even  $\text{C}_3$  and  $\text{C}_4$  products of  $\text{C}_3\text{H}_7\text{OH}$ ,  $\text{C}_3\text{H}_6$ ,  $\text{C}_3\text{H}_8$ ,  $\text{C}_4\text{H}_{10}$  were observed from Cl ion-adsorbed oxide-derived Cu [173]. Oxide-derived Sn showed much higher current density and faraday efficiency than a pristine Sn electrode for formic acid production [128, 133]. Oxide-derived Au [174] or Ag [175] showed superior faraday efficiency for CO production, with 90 ~ 100% at only 0.3 V overpotential, as shown in Fig. 11a.

There have been debates on the origin of the enhancement of oxide-derived metal for  $\text{CO}_2\text{RR}$ . Nano-structures induced in the catalysts or residual subsurface oxygen have been suggested as the source of the enhancement. Nano-structured surfaces with rich grain boundaries were obtained after oxidation-reduction cycling [176, 177]. The induced surface had more defect sites with higher binding energy to  $^*\text{CO}$  and higher local pH which increased



selectivity toward CO<sub>2</sub>RR while suppressing HER [169, 176–178]. It was also suggested that some oxygen remained in the subsurface despite the highly reducing conditions of the CO<sub>2</sub>RR. Ambient pressure XPS, in situ electron energy loss spectroscopy (EELS) experiments, and DFT calculations showed that the oxygen helped to activate CO<sub>2</sub> on the surface in the initial step, as shown in Fig. 11b [179, 180]. However, a contradictory result was also reported, saying that the residual oxide was very unstable in the CO<sub>2</sub>RR condition, and that the amount of oxygen was negligible [181].

#### Alloy metals

By alloying with a secondary metal, the intrinsic catalytic performance of metal can be modified, and high selectivity or activity can be obtained for CO<sub>2</sub>RR [101, 127]. The enhancement was typically attributed to an electronic or geometric effect on the alloyed catalysts [101, 127]. The presence of a secondary metal led to modulation in the electronic structure of the active site. The binding energy between the active site and reaction intermediate could be tuned, changing the reaction pathway and the resulting selectivity [182–185]. The secondary metal can also change the surface geometric structure, with different atomic arrangements of reactant or intermediates. The electronic and geometric effect has been systematically studied for Au-Cu bimetallic nanoparticle catalysts with different compositions [183, 184]. Figure 12a shows that the *d*-band center was downshifted as Au content increased, and the change in the electronic structure lowered the binding energy of \*COOH and \*CO. The Cu atom was bound to the oxygen end of the \*COOH, while the Au atom formed a Au-C bond [183]. The binding strength of each primary bond and the adsorption configuration were tailored by changing the composition of the bimetallic particles. The ordered Au-Cu with three atomic overlayers of Au showed high performance for CO production due to the

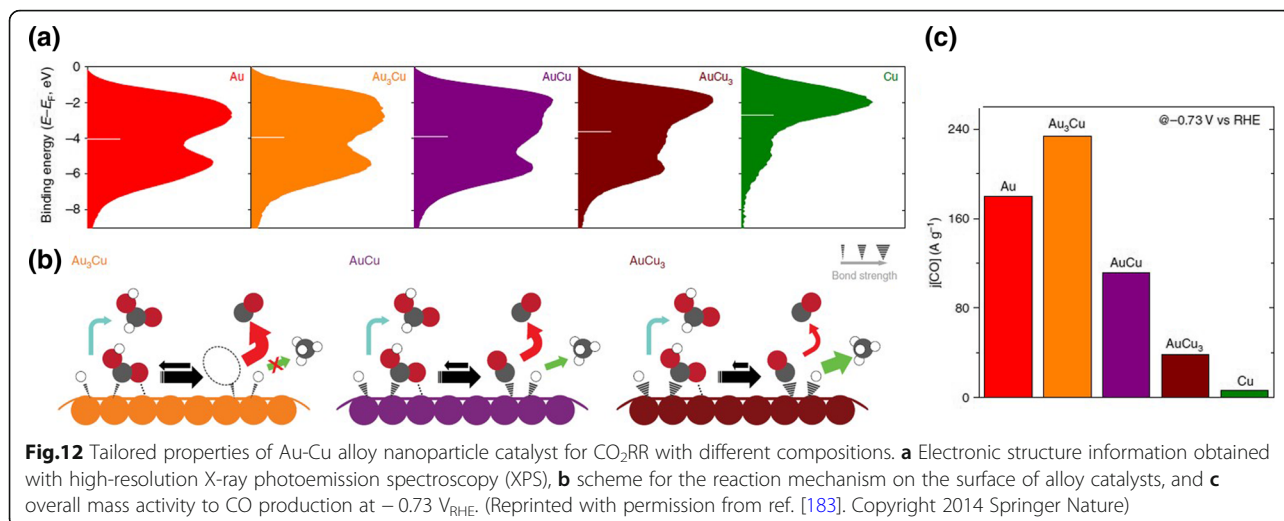
change in binding energy induced by atomic strains [184]. The reaction path to the C-C coupling was suppressed by the geometric property of the ordered Au<sub>3</sub>Cu alloys, producing CH<sub>4</sub> [185].

The alloy catalysts deviate from the general scaling relationship of binding strength to intermediates, and by controlling mixing patterns, they can exhibit unique selectivity. For example, while ordered Cu-Pd nanoparticles selectively produced C<sub>1</sub> products, mainly CO, but phase-separated Cu-Pd nanoparticles produced C<sub>2</sub> products, mainly C<sub>2</sub>H<sub>4</sub> [185]. Cu ensemble sites were needed to make C-C bonds, and neighboring Pd sites further helped hydrogenation by hydrogen spillover.

For multi-electron paths rather than a two-electron path, the key intermediates of \*CHO or \*COH should be formed, but proton-coupled electron transfer on \*CO to form \*CHO or \*COH is a rate determining step [101]. It was reported that if Cu was alloyed with a metal that could stabilize O, the adsorption configuration of \*CHO or \*COH on the Cu-M sites could be adjusted and their formation would be favored [186]. Consequently, the overpotential for further reduction decreased and the selectivity of CO<sub>2</sub>RR could be controlled. Many other alloy catalysts were reported for CO<sub>2</sub>RR; Cu-In [187], Cu-Sn [188] for CO production, Pd-Pt [189], Ag-Sn [190], Sn-Pb [191], Sn-Pd [192], Au-Pd [193] for formate production.

#### Carbon-based materials

Carbon-based materials have been actively studied as promising electrocatalysts for electrochemical reactions, such as the oxygen reduction reaction (ORR), OER, and HER [194, 195]. Carbon materials have advantages for electrochemical applications, including facile transformability to various dimensions and shapes [196]. Zero-dimensional carbon dots or graphene quantum dots, one-dimensional carbon nanotubes, two-dimensional



graphene, and three-dimensional graphene aerogel can be produced with well-developed material science techniques [97]. The carbon materials also possess high conductivity, high surface area, and good chemical and mechanical stability.

Pure carbon materials are basically inert toward CO<sub>2</sub>RR. However, if heteroatoms such as N are doped in the carbon matrix, electrocatalytic activity is greatly enhanced. Negatively charged N sites are considered active sites for CO<sub>2</sub>RR [197–199]. N-doping introduces a Lewis base site to the catalyst, which is beneficial to stabilize CO<sub>2</sub> [196, 197]. Various carbon materials, including N-doped carbon nanotubes [200, 201], N-doped graphenes [202], N-doped graphene quantum dots [203] were reported for CO<sub>2</sub>RR following the two-electron pathway. N-doped diamond produced acetate as well as formate with N-sp<sup>3</sup>C active sites [204]. Other dopants such as S or B have also been used for CO<sub>2</sub>RR [205, 206].

### Single atom catalysts

Single atom catalysts (SAC) represent atomically dispersed metal catalysts on the surface of a support. They exhibit very distinct electronic structures and adsorption configurations of reactants and intermediates, with unique selectivity [207]. SACs have been used for electrochemical ORR [208, 209], HER [210], formic acid oxidation reaction (FAOR) [211], and CO<sub>2</sub>RR [212]. Ni single atoms on N-doped graphene can catalyze CO<sub>2</sub>RR producing CO selectively, as shown in Fig. 13 [212]. Other metal atoms of Fe, Co, Mn, and Cu with slightly different *d*-band structure have shown different selectivity. The coordination environment neighboring the Ni single atom has also been reported to affect the electronic structure and the binding energy of key carbon intermediates [213, 214]. When Cu was atomically

doped into CeO<sub>2</sub>, the oxygen defect sites of the CeO<sub>2</sub> regulated the oxidation state of Cu by forming Cu ion-O vacancy pairs. The single atomic Cu catalyzed CO<sub>2</sub>RR, producing CH<sub>4</sub> with 58% faraday efficiency [215]. DFT calculations have also predicted that the SAC structure can suppress HER while promoting CO<sub>2</sub>RR, with the proper choice of metal atom and supports [216, 217]. Single atom alloys where a single atomic metal is located on another metal surface have also been suggested by computational method as efficient catalysts for CO<sub>2</sub>RR [218].

Although many intensive efforts have been dedicated to develop electrochemical CO<sub>2</sub>RR, the performance is still far from the performance obtained from gas-phase CO<sub>2</sub> reduction. To enhance electrochemical CO<sub>2</sub>RR further, various other efforts have been tried, by tuning other factors. Electrolyte compositions, pH, and concentrations affected activity and selectivity [96, 219–222]. Ionic liquids helped the activation of CO<sub>2</sub> [223, 224]. An electric field near the electrode was shown to stabilize charged intermediates better [113, 220]. The additives could control selectivity via electron shuttling or the formation of surface films [225, 226]. A gas diffusion electrode (GDE) cell allowed unprecedentedly high current density [171, 227]. Stability, resistivity to catalyst poisons, and activity on diluted CO<sub>2</sub> feed are also important for practical applications, but they have not yet attracted much interest at this stage. To develop this technology to a commercially feasible level, those many factors should be optimized.

### Conclusion and perspectives

Heterogeneous catalysts used for catalytic CO<sub>2</sub> conversion into valuable chemicals such as CO, CH<sub>4</sub>, C<sub>2</sub>H<sub>4</sub> have been discussed in this review. Because CO<sub>2</sub> is thermodynamically very stable, its conversion usually

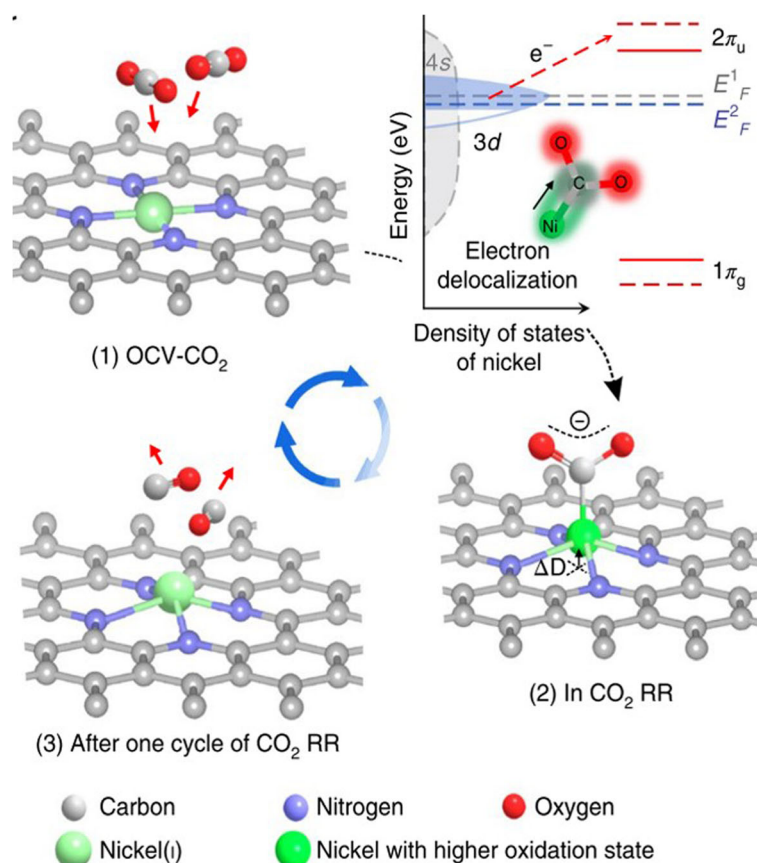


**Fig. 13** Structural evolution of Ni single-atom sites on graphene during CO<sub>2</sub>RR (Reprinted with permission from ref. [212]. Copyright 2018 Springer Nature)

requires a lot of energy, but the production of that energy also emits considerable CO<sub>2</sub>. Obtaining negative net CO<sub>2</sub> emissions is not easy, and the design of efficient catalysts for CO<sub>2</sub> conversion is a key to reducing CO<sub>2</sub> emissions.

Catalytic CO<sub>2</sub> conversion can occur in gas-phase, liquid-phase, or electrochemical cells. Because the solubility of CO<sub>2</sub> is quite low in aqueous solution, the CO<sub>2</sub> conversion in liquid-phase typically suffer from low productivity. Thus this review mainly focused on the conversion using gaseous CO<sub>2</sub>. Various metals, metal oxides, metal carbides, and doped carbon materials have been used as catalysts for CO<sub>2</sub> conversion. Synthetic strategies have been developed to endure high reaction temperatures and minimize coke formation for dry methane reforming. The CO<sub>2</sub> hydrogenation can be efficient, but they use H<sub>2</sub> gas. The H<sub>2</sub> gas is conventionally produced from methane steam reforming, which also produces considerable CO<sub>2</sub>. If H<sub>2</sub> can be produced from water without CO<sub>2</sub> emissions, CO<sub>2</sub> hydrogenation in gas-phase would be a very powerful tool for efficient CO<sub>2</sub> conversion. The gaseous product of CO or CH<sub>4</sub> have been mainly considered as products from the CO<sub>2</sub> hydrogenation, but liquid products such as formic acid

or dimethyl ether would also have high value. Metal-based catalysts including precious metal or supported Ni catalysts have been used for the production of CO or CH<sub>4</sub>. Not many good heterogeneous catalysts have been found for the production of formic acid, instead homogeneous catalysts have been typically used. Robust heterogeneous catalyst producing formic acid might have high potential. Catalysts that use both heat and light as energy sources have been developed, to minimize total energy use.

Electrochemical CO<sub>2</sub> conversion has shown improved productivity using gas-diffusion electrode cells. It is also very promising because it directly uses CO<sub>2</sub> and H<sub>2</sub>O for chemical or fuel production. The technology for electrochemical CO<sub>2</sub> reduction is in its early stages, compared to other CO<sub>2</sub> conversion technologies, but it is being investigated very actively. A variety of materials have been tested as catalysts for electrochemical CO<sub>2</sub> reduction, and the catalysts should be tuned depending on the target products. Au or Ag produces CO, Sn or Bi produces formate, and Cu produces hydrocarbons such as C<sub>2</sub>H<sub>4</sub>. Considering the cell design of gas-diffusion electrodes, nano-structured catalysts should be optimized further. Most studies so far have used concentrated pure CO<sub>2</sub>

for the conversion. But the conversion of dilute CO<sub>2</sub>, especially in the presence of potential catalyst poisons such as S compounds, should be investigated more actively for practical applications.

#### Abbreviations

CO<sub>2</sub>RR: Electrochemical CO<sub>2</sub> reduction reaction; DFT: Density functional theory; DRM: Dry reforming of methane; EELS: Electron energy loss spectroscopy; EXAFS: Extended X-ray absorption fine structure; GDE: Gas diffusion electrode; HER: Hydrogen evolution reaction; OER: Oxygen evolution reaction; ORR: Oxygen reduction reaction; POM: Partial oxidation of methane; RHE: Reversible hydrogen electrode; RWGS: Reverse water gas shift; SAC: Single atom catalysts; SMSI: Strong-metal support interaction; SRM: Steam reforming of methane; TMC: Transition-metal carbide; XAFS: X-ray absorption fine structure; XANES: X-ray absorption near edge structure

#### Acknowledgements

Not applicable

#### Funding

This work was financially supported by the National Research Foundation of Korea (NRF-2017M3D1A1040692) funded by the Ministry of Education, Science and Technology and the Saudi Aramco-KAIST CO<sub>2</sub> Management Center.

#### Availability of data and materials

Not applicable

#### Authors' contributions

HL organized the overall structure. HSW wrote the manuscript about DRM, MSC wrote the manuscript about RWGS, JLee wrote the manuscript about light-assisted CO<sub>2</sub> hydrogenation, JLim wrote the manuscript about CO<sub>2</sub>RR. All authors read and approved the final manuscript.

#### Competing interests

The authors declare that they have no competing interests.

#### Publisher's Note

Springer Nature remains neutral with regard to jurisdictional claims in published maps and institutional affiliations.

Received: 1 November 2018 Accepted: 22 February 2019

Published online: 27 March 2019

#### References

- Hansen J, Ruedy R, Sato M, Lo K. Global surface temperature change. *Rev Geophys*. 2010;48:RG4004.
- Dincer I. Renewable energy and sustainable development: a crucial review. *Renew Sust Energ Rev*. 2000;4(2):157–75.
- Burke MJ, Stephens JC. Political power and renewable energy futures: a critical review. *Energy Res Soc Sci*. 2018;35:78–93.
- Alvarez A, Bansode A, Urakawa A, Bavykina AV, Wezendonk TA, Makkee M, Gascon J, Kaptejin F. Challenges in the greener production of formates/formic acid, methanol, and DME by heterogeneously catalyzed CO<sub>2</sub> hydrogenation processes. *Chem Rev*. 2017;117(14):9804–38.
- Lim RJ, Xie M, Sk MA, Lee J-M, Fisher A, Wang X, Lim KH. A review on the electrochemical reduction of CO<sub>2</sub> in fuel cells, metal electrodes and molecular catalysts. *Catal Today*. 2014;233:169–80.
- Porosoff MD, Yan B, Chen JG. Catalytic reduction of CO<sub>2</sub> by H<sub>2</sub> for synthesis of CO, methanol and hydrocarbons: challenges and opportunities. *Energy Environ Sci*. 2016;9(1):62–73.
- Yan N, Philippot K. Transformation of CO<sub>2</sub> by using nanoscale metal catalysts: cases studies on the formation of formic acid and dimethylether. *Curr Opin Chem Eng*. 2018;20:86–92.
- Wang WH, Himeda Y, Muckerman JT, Manbeck GF, Fujita E. CO<sub>2</sub> hydrogenation to formate and methanol as an alternative to photo- and electrochemical CO<sub>2</sub> reduction. *Chem Rev*. 2015;115(23):12936–73.
- Li WH, Wang HZ, Jiang X, Zhu J, Liu ZM, Guo XW, Song CS. A short review of recent advances in CO<sub>2</sub> hydrogenation to hydrocarbons over heterogeneous catalysts. *RSC Adv*. 2018;8(14):7651–69.
- Li K, Peng BS, Peng TY. Recent advances in heterogeneous photocatalytic CO<sub>2</sub> conversion to solar fuels. *ACS Catal*. 2016;6(11):7485–527.
- Gunasekar GH, Park K, Jung KD, Yoon S. Recent developments in the catalytic hydrogenation of CO<sub>2</sub> to formic acid/formate using heterogeneous catalysts. *Inorg Chem Front*. 2016;3(7):882–95.
- Kawi S, Kathiraser Y, Ni J, Oemar U, Li ZW, Saw ET. Progress in synthesis of highly active and stable nickel-based catalysts for carbon dioxide reforming of methane. *ChemSusChem*. 2015;8(21):3556–75.
- Pakhare D, Spivey J. A review of dry (CO<sub>2</sub>) reforming of methane over noble metal catalysts. *Chem Soc Rev*. 2014;43(22):7813–37.
- York APE, Xiao TC, Green MLH. Brief overview of the partial oxidation of methane to synthesis gas. *Top Catal*. 2003;22(3–4):345–58.
- Kim HY, Park JN, Henkelman G, Kim JM. Design of a highly nanodispersed Pd-MgO/SiO<sub>2</sub> composite catalyst with multifunctional activity for CH<sub>4</sub> reforming. *ChemSusChem*. 2012;5(8):1474–81.
- Gallego GS, Batiot-Dupeyrat C, Barrault J, Florez E, Mondragon F. Dry reforming of methane over LaNi<sub>1-x</sub>B<sub>x</sub>O<sub>3+/-delta</sub> (B=Mg, Co) perovskites used as catalyst precursor. *Appl Catal A*. 2008;334(1–2):251–8.
- Pakhare D, Shaw C, Haynes D, Shekhawat D, Spivey J. Effect of reaction temperature on activity of Pt- and Ru-substituted lanthanum zirconate pyrochlores (La<sub>2</sub>Zr<sub>2</sub>O<sub>7</sub>) for dry (CO<sub>2</sub>) reforming of methane (DRM). *J CO<sub>2</sub> Util*. 2013;1:37–42.
- Bian ZF, Das S, Wai MH, Hongmanorom P, Kawi S. A review on bimetallic nickel-based catalysts for CO<sub>2</sub> reforming of methane. *ChemPhysChem*. 2017;18(22):3117–34.
- Arora S, Prasad R. An overview on dry reforming of methane: strategies to reduce carbonaceous deactivation of catalysts. *RSC Adv*. 2016;6(110):108668–88.
- Aramouni NAK, Touma JG, Abu Tarboush B, Zeaiter J, Ahmad MN. Catalyst design for dry reforming of methane: analysis review. *Renew Sust Energ Rev*. 2018;82:2570–85.
- Wang SB, Lu GQM, Millar GJ. Carbon dioxide reforming of methane to produce synthesis gas over metal-supported catalysts: state of the art. *Energy Fuel*. 1996;10(4):896–904.
- Kambolis A, Matralis H, Trovarelli A, Papadopoulou C. Ni/CeO<sub>2</sub>-ZrO<sub>2</sub> catalysts for the dry reforming of methane. *Appl Catal A*. 2010;377(1–2):16–26.
- Sutthiumporn K, Maneerung T, Kathiraser Y, Kawi S. CO<sub>2</sub> dry-reforming of methane over La<sub>0.8</sub>Sr<sub>0.2</sub>Ni<sub>0.8</sub>Mn<sub>0.2</sub>O<sub>3</sub> perovskite (M = Bi, Co, Cr, Cu, Fe): roles of lattice oxygen on C-H activation and carbon suppression. *Int J Hydrog Energy*. 2012;37(15):11195–207.
- Bhavani AG, Kim WY, Lee JS. Barium substituted lanthanum manganite perovskite for CO<sub>2</sub> reforming of methane. *ACS Catal*. 2013;3(7):1537–44.
- Hu YH. Solid-solution catalysts for CO<sub>2</sub> reforming of methane. *Catal Today*. 2009;148(3–4):206–11.
- Zanganeh R, Rezaei M, Zamaniyan A. Dry reforming of methane to synthesis gas on NiO-MgO nanocrystalline solid solution catalysts. *Int J Hydrog Energy*. 2013;38(7):3012–8.
- Garcia-Dieguez M, Pieta IS, Herrera MC, Larrubia MA, Malpartida I, Alemany LJ. Transient study of the dry reforming of methane over Pt supported on different gamma-Al<sub>2</sub>O<sub>3</sub>. *Catal Today*. 2010;149(3–4):380–7.
- Yokota S, Okumura K, Niwa M. Support effect of metal oxide on Rh catalysts in the CH<sub>4</sub>-CO<sub>2</sub> reforming reaction. *Catal Lett*. 2002;84(1–2):131–4.
- Menad S, Ferreira-Aparicio P, Cherifi O, Guerrero-Ruiz A, Rodriguez-Ramos I. Designing new high oxygen mobility supports to improve the stability of Ru catalysts under dry reforming of methane. *Catal Lett*. 2003;89(1–2):63–7.
- Ferreira-Aparicio P, Guerrero-Ruiz A, Rodriguez-Ramos I. Comparative study at low and medium reaction temperatures of syngas production by methane reforming with carbon dioxide over silica and alumina supported catalysts. *Appl Catal A*. 1998;170(1):177–87.
- Whang HS, Choi MS, Lim J, Kim C, Heo I, Chang TS, Lee H. Enhanced activity and durability of Ru catalyst dispersed on zirconia for dry reforming of methane. *Catal Today*. 2017;293:122–8.
- Park J-H, Yeo S, Heo I, Chang T-S. Promotional effect of Al addition on the Co/ZrO<sub>2</sub> catalyst for dry reforming of CH<sub>4</sub>. *Appl Catal A*. 2018;562:120.
- Park J-H, Yeo S, Kang T-J, Heo I, Lee K-Y, Chang T-S. Enhanced stability of Co catalysts supported on phosphorus-modified Al<sub>2</sub>O<sub>3</sub> for dry reforming of CH<sub>4</sub>. *Fuel*. 2018;212:77–87.
- Ay H, Uner D. Dry reforming of methane over CeO<sub>2</sub> supported Ni, Co and Ni-Co catalysts. *Appl Catal B*. 2015;179:128–38.
- Miura H, Endo K, Ogawa R, Shishido T. Supported palladium-gold alloy catalysts for efficient and selective hydrosilylation under mild conditions

- with isolated single palladium atoms in alloy nanoparticles as the main active site. *ACS Catal.* 2017;7(3):1543–53.
36. Kim SM, Abdala PM, Margossian T, Hosseini D, Foppa L, Armutulu A, van Beek W, Comas-Vives A, Coperet C, Muller C. Cooperativity and dynamics increase the performance of NiFe dry reforming catalysts. *J Am Chem Soc.* 2017;139(5):1937–49.
  37. Nakamura J, Aikawa K, Sato K, Uchijima T. Role of support in reforming of CH<sub>4</sub> with CO<sub>2</sub> over Rh catalysts. *Catal Lett.* 1994;25(3–4):265–70.
  38. Liu DP, Quek XY, Cheo WNE, Lau R, Borgna A, Yang YH. MCM-41 supported nickel-based bimetallic catalysts with superior stability during carbon dioxide reforming of methane: effect of strong metal-support interaction. *J Catal.* 2009;266(2):380–90.
  39. Guo JJ, Lou H, Zhao H, Chai DF, Zheng XM. Dry reforming of methane over nickel catalysts supported on magnesium aluminate spinels. *Appl Catal A.* 2004;273(1–2):75–82.
  40. Ferreira-Aparicio P, Rodriguez-Ramos I, Anderson JA, Guerrero-Ruiz A. Mechanistic aspects of the dry reforming of methane over ruthenium catalysts. *Appl Catal A.* 2000;202(2):183–96.
  41. Zhang ZL, Veykios XE, MacDonald SM, Affrossman S. Comparative study of carbon dioxide reforming of methane to synthesis gas over Ni/La<sub>2</sub>O<sub>3</sub> and conventional nickel-based catalysts. *J Phys Chem.* 1996;100(2):744–54.
  42. Alipour Z, Rezaei M, Meshkani F. Effect of alkaline earth promoters (MgO, CaO, and BaO) on the activity and coke formation of Ni catalysts supported on nanocrystalline Al<sub>2</sub>O<sub>3</sub> in dry reforming of methane. *Ind Eng Chem Res.* 2014;20(5):2858–63.
  43. Bellido JDA, De Souza JE, M'Peko JC, Assaf EM. Effect of adding CaO to ZrO<sub>2</sub> support on nickel catalyst activity in dry reforming of methane. *Appl Catal A.* 2009;358(2):215–23.
  44. Pechimuthu NA, Pant KK, Dhingra SC, Bhalla R. Characterization and activity of K, CeO<sub>2</sub>, and Mn promoted Ni/Al<sub>2</sub>O<sub>3</sub> catalysts for carbon dioxide reforming of methane. *Ind Eng Chem Res.* 2006;45(22):7435–43.
  45. Therdtianwong S, Therdtianwong A, SiangChin C, Yonprapat S. Synthesis gas production from dry reforming of methane over Ni/Al<sub>2</sub>O<sub>3</sub> stabilized by ZrO<sub>2</sub>. *Int J Hydrog Energy.* 2008;33(3):991–9.
  46. Laosiripojana N, Sutthiripok W, Assabumrungrat S. Synthesis gas production from dry reforming of methane over CeO<sub>2</sub> doped Ni/Al<sub>2</sub>O<sub>3</sub>: influence of the doping ceria on the resistance toward carbon formation. *Chem Eng J.* 2005; 112(1–3):13–22.
  47. Liang TY, Lin CY, Chou FC, Wang MQ, Tsai DH. Gas-phase synthesis of Ni-CeO<sub>x</sub> hybrid nanoparticles and their synergistic catalysis for simultaneous reforming of methane and carbon dioxide to syngas. *J Phys Chem C.* 2018; 122(22):11789–98.
  48. Bellido JDA, Assaf EM. Effect of the Y<sub>2</sub>O<sub>3</sub>-ZrO<sub>2</sub> support composition on nickel catalyst evaluated in dry reforming of methane. *Appl Catal A.* 2009; 352(1–2):179–87.
  49. Wang N, Chu W, Zhang T, Zhao XS. Synthesis, characterization and catalytic performances of Ce-SBA-15 supported nickel catalysts for methane dry reforming to hydrogen and syngas. *Int J Hydrog Energy.* 2012;37(1):19–30.
  50. Damyanova S, Pawelec B, Arishtirova K, Huerta MVM, Fierro JLG. The effect of CeO<sub>2</sub> on the surface and catalytic properties of Pt/CeO<sub>2</sub>-ZrO<sub>2</sub> catalysts for methane dry reforming. *Appl Catal B.* 2009;89(1–2):149–59.
  51. Zhu YA, Chen D, Zhou XG, Yuan WK. DFT studies of dry reforming of methane on Ni catalyst. *Catal Today.* 2009;148(3–4):260–7.
  52. Ni J, Chen LW, Lin JY, Kawi S. Carbon deposition on borated alumina supported nano-sized Ni catalysts for dry reforming of CH<sub>4</sub>. *Nano Energy.* 2012;1(5):674–86.
  53. Han JW, Kim C, Park JS, Lee H. Highly coke-resistant Ni nanoparticle catalysts with minimal sintering in dry reforming of methane. *ChemSusChem.* 2014;7(2):451–6.
  54. Lu JL, Fu BS, Kung MC, Xiao GM, Elam JW, Kung HH, Stair PC. Coking- and sintering-resistant palladium catalysts achieved through atomic layer deposition. *Science.* 2012;335(6073):1205–8.
  55. Han JW, Park JS, Choi MS, Lee H. Uncoupling the size and support effects of Ni catalysts for dry reforming of methane. *Appl Catal B.* 2017;203:625–32.
  56. Gould TD, Izar A, Weimer AW, Falconer JL, Medlin JW. Stabilizing Ni catalysts by molecular layer deposition for harsh, dry reforming conditions. *ACS Catal.* 2014;4(8):2714–7.
  57. Das S, Ashok J, Bian Z, Dewangan N, Wai MH, Du Y, Borgna A, Hidajat K, Kawi S. Silica-ceria sandwiched Ni core-shell catalyst for low temperature dry reforming of biogas: coke resistance and mechanistic insights. *Appl Catal B.* 2018;230:220–36.
  58. Song H. Metal hybrid nanoparticles for catalytic organic and photochemical transformations. *Acc Chem Res.* 2015;48(3):491–9.
  59. Chaudhuri RG, Paria S. Core/shell nanoparticles: classes, properties, synthesis mechanisms, characterization, and applications. *Chem Rev.* 2012;112(4):2373–433.
  60. Cargnello M, Jaen JJD, Garrido JCH, Bakhmutsky K, Montini T, Gamez JJC, Gorte RJ, Fornasiero P. Exceptional activity for methane combustion over modular Pd@CeO<sub>2</sub> subunits on functionalized Al<sub>2</sub>O<sub>3</sub>. *Science.* 2012; 337(6095):713–7.
  61. Joo SH, Park JY, Tsung CK, Yamada Y, Yang PD, Somorjai GA. Thermally stable Pt/mesoporous silica core-shell nanocatalysts for high-temperature reactions. *Nat Mater.* 2009;8(2):126–31.
  62. Li ZW, Mo LY, Kathiraser Y, Kawi S. Yolk-satellite-shell structured Ni-Yolk@Ni@SiO<sub>2</sub> nanocomposite: superb catalyst toward methane CO<sub>2</sub> reforming reaction. *ACS Catal.* 2014;4(5):1526–36.
  63. Wang K, Li XJ, Ji SF, Shi XJ, Tang JJ. Effect of Ce<sub>x</sub>Zr<sub>1-x</sub>O<sub>2</sub> promoter on Ni-based SBA-15 catalyst for steam reforming of methane. *Energy Fuel.* 2009;23(1–2):25–31.
  64. Joo SH, Choi SJ, Oh I, Kwak J, Liu Z, Terasaki O, Ryoo R. Ordered nanoporous arrays of carbon supporting high dispersions of platinum nanoparticles. *Nature.* 2001;412(6843):169–72.
  65. Wu Z, Li Q, Feng D, Webley PA, Zhao D. Ordered mesoporous crystalline γ-Al<sub>2</sub>O<sub>3</sub> with variable architecture and porosity from a single hard template. *J Am Chem Soc.* 2010;132(34):12042–50.
  66. Yuan Q, Yin A-X, Luo C, Sun L-D, Zhang Y-W, Duan W-T, Liu H-C, Yan C-H. Facile synthesis for ordered mesoporous γ-aluminas with high thermal stability. *J Am Chem Soc.* 2008;130(11):3465–72.
  67. Wang N, Shen K, Huang LH, Yu XP, Qian WZ, Chu W. Facile route for synthesizing ordered mesoporous Ni-Ce-Al oxide materials and their catalytic performance for methane dry reforming to hydrogen and syngas. *ACS Catal.* 2013;3(7):1638–51.
  68. Bosch C, Wild W. Producing hydrogen. In: Google patents; 1914.
  69. Fang KG, Li DB, Lin MG, Xiang ML, Wei W, Sun YH. A short review of heterogeneous catalytic process for mixed alcohols synthesis via syngas. *Catal Today.* 2009;147(2):133–8.
  70. Gao JJ, Wang YL, Ping Y, Hu DC, Xu GW, Gu FN, Su FB. A thermodynamic analysis of methanation reactions of carbon oxides for the production of synthetic natural gas. *RSC Adv.* 2012;2(6):2358–68.
  71. Gines MJL, Marchi AJ, Apesteguia CR. Kinetic study of the reverse water-gas shift reaction over CuO/ZnO/Al<sub>2</sub>O<sub>3</sub> catalysts. *Appl Catal A.* 1997;154(1–2):155–71.
  72. Chen CS, Cheng WH, Lin SS. Mechanism of CO formation in reverse water-gas shift reaction over Cu/Al<sub>2</sub>O<sub>3</sub> catalyst. *Catal Lett.* 2000;68(1–2):45–8.
  73. Chen XD, Su X, Duan HM, Liang BL, Huang YQ, Zhang T. Catalytic performance of the Pt/TiO<sub>2</sub> catalysts in reverse water gas shift reaction: controlled product selectivity and a mechanism study. *Catal Today.* 2017;281:312–8.
  74. Xu HT, Li YS, Luo XK, Xu ZL, Ge JP. Monodispersed gold nanoparticles supported on a zirconium-based porous metal-organic framework and their high catalytic ability for the reverse water-gas shift reaction. *Chem Commun.* 2017;53(56):7953–6.
  75. Ye J, Ge Q, Liu CJ. Effect of PdIn bimetallic particle formation on CO<sub>2</sub> reduction over the Pd-In/SiO<sub>2</sub> catalyst. *Chem Eng Sci.* 2015;135:193–201.
  76. Goncalves RV, Vono LLR, Wojcieszak R, Dias CSB, Wender H, Teixeira-Neto E, Rossi LM. Selective hydrogenation of CO<sub>2</sub> into CO on a highly dispersed nickel catalyst obtained by magnetron sputtering deposition: a step towards liquid fuels. *Appl Catal B.* 2017;209:240–6.
  77. Sun FM, Yan CF, Wang ZD, Guo CQ, Huang SL. Ni/Ce-Zr-O catalyst for high CO<sub>2</sub> conversion during reverse water gas shift reaction (RWGS). *Int J Hydrog Energy.* 2015;40(46):15985–93.
  78. Galvan CA, Schumann J, Behrens M, Fierro JLG, Schlögl R, Frei E. Reverse water-gas shift reaction at the Cu/ZnO interface: influence of the Cu/Zn ratio on structure-activity correlations. *Appl Catal B.* 2016;195:104–11.
  79. Zhou GL, Dai BC, Xie HM, Zhang GZ, Xiong K, Zheng XX. CeCu composite catalyst for CO synthesis by reverse water-gas shift reaction: effect of Ce/Cu mole ratio. *J CO<sub>2</sub> UTIL.* 2017;21:292–301.
  80. Porosoff MD, Kattel S, Li WH, Liu P, Chen JG. Identifying trends and descriptors for selective CO<sub>2</sub> conversion to CO over transition metal carbides. *Chem Commun.* 2015;51(32):6988–91.
  81. Porosoff MD, Baldwin JW, Peng X, Mpourmpakis G, Willauer HD. Potassium-promoted molybdenum carbide as a highly active and selective catalyst for CO<sub>2</sub> conversion to CO. *ChemSusChem.* 2017;10(11):2408–15.
  82. Liu XY, Kunkel C, de la Piscina PR, Homs N, Vines F, Illas F. Effective and highly selective CO generation from CO<sub>2</sub> using a polycrystalline alpha-Mo<sub>2</sub>C catalyst. *ACS Catal.* 2017;7(7):4323–35.

83. Zhang X, Zhu XB, Lin LL, Yao SY, Zhang MT, Liu X, Wang XP, Li YW, Shi C, Ma D. Highly dispersed copper over beta-Mo<sub>2</sub>C as an efficient and stable catalyst for the reverse water gas shift (RWGS) reaction. *ACS Catal.* 2017;7(1):912–8.
84. Wu JJ, Wen C, Zou XL, Jimenez J, Sun J, Xia YJ, Rodrigues MTF, Vinod S, Zhong J, Chopra N, et al. Carbon dioxide hydrogenation over a metal-free carbon-based catalyst. *ACS Catal.* 2017;7(7):4497–503.
85. Frontera P, Macario A, Ferraro M, Antonucci P. Supported catalysts for CO<sub>2</sub> methanation: a review. *Catalysts.* 2017;7(2):59.
86. Arandiyani H, Wang Y, Sun HY, Rezaei M, Dai HX. Ordered meso- and macroporous perovskite oxide catalysts for emerging applications. *Chem Commun.* 2018;54(50):6484–502.
87. Arandiyani H, Wang Y, Scott J, Mesgari S, Dai HX, Amal R. In situ exsolution of bimetallic Rh-Ni nanoalloys: a highly efficient catalyst for CO<sub>2</sub> methanation. *ACS Appl Mater Interfaces.* 2018;10(19):16352–7.
88. Wang Y, Arandiyani H, Scott J, Dai HX, Amal R. Hierarchically porous network-like Ni/Co<sub>3</sub>O<sub>4</sub>: noble metal-free catalysts for carbon dioxide methanation. *Adv Sustain Syst.* 2018;2(3):1700119.
89. Chang X, Wang T, Gong J. CO<sub>2</sub> photo-reduction: insights into CO<sub>2</sub> activation and reaction on surfaces of photocatalysts. *Energy Environ Sci.* 2016;9(7):2177–96.
90. Neaţu S, Maciá-Agulló JA, Concepción P, García H. Gold–copper nanoalloys supported on TiO<sub>2</sub> as photocatalysts for CO<sub>2</sub> reduction by water. *J Am Chem Soc.* 2014;136(45):15969–76.
91. Huang M, Fabris S. CO adsorption and oxidation on ceria surfaces from DFT+U calculations. *J Phys Chem C.* 2008;112(23):8643–8.
92. Kale MJ, Avanesian T, Xin H, Yan J, Christopher P. Controlling catalytic selectivity on metal nanoparticles by direct photoexcitation of adsorbate–metal bonds. *Nano Lett.* 2014;14(9):5405–12.
93. Lindstrom C, Zhu X-Y. Photoinduced electron transfer at molecule–metal interfaces. *Chem Rev.* 2006;106(10):4281–300.
94. Kim C, Hyeon S, Lee J, Kim WD, Lee DC, Kim J, Lee H. Energy-efficient CO<sub>2</sub> hydrogenation with fast response using photoexcitation of CO<sub>2</sub> adsorbed on metal catalysts. *Nat Commun.* 2018;9(1):3027.
95. Zhu DD, Liu JL, Qiao SZ. Recent advances in inorganic heterogeneous electrocatalysts for reduction of carbon dioxide. *Adv Mater.* 2016;28(18):3423–52.
96. Singh MR, Clark EL, Bell AT. Effects of electrolyte, catalyst, and membrane composition and operating conditions on the performance of solar-driven electrochemical reduction of carbon dioxide. *Phys Chem Chem Phys.* 2015;17(29):18924–36.
97. Vasileff A, Zheng Y, Qiao SZ. Carbon solving carbon's problems: recent progress of nanostructured carbon-based catalysts for the electrochemical reduction of CO<sub>2</sub>. *Adv Eng Mater.* 2017;7(21):1700759.
98. Seh ZW, Kibsgaard J, Dickens CF, Chorkendorff IB, Norskov JK, Jaramillo TF. Combining theory and experiment in electrocatalysis: insights into materials design. *Science.* 2017;355(6321):4998.
99. Bushuyev OS, De Luna P, Dinh CT, Tao L, Saur G, van de Lagemaat J, Kelley SO, Sargent EH. What should we make with CO<sub>2</sub> and how can we make it? *Joule.* 2018;2(5):825–32.
100. Wang YH, Liu JL, Wang YF, Al-Enizi AM, Zheng GF. Tuning of CO<sub>2</sub> reduction selectivity on metal electrocatalysts. *Small.* 2017;13(43):1701809.
101. Vasileff A, Xu CC, Jiao Y, Zheng Y, Qiao SZ. Surface and interface engineering in copper-based bimetallic materials for selective CO<sub>2</sub> electroreduction. *Chem.* 2018;4(8):1809–31.
102. Kuhl KP, Hatsukade T, Cave ER, Abram DN, Kibsgaard J, Jaramillo TF. Electrocatalytic conversion of carbon dioxide to methane and methanol on transition metal surfaces. *J Am Chem Soc.* 2014;136(40):14107–13.
103. Feaster JT, Shi C, Cave ER, Hatsukade TT, Abram DN, Kuhl KP, Hahn C, Norskov JK, Jaramillo TF. Understanding selectivity for the electrochemical reduction of carbon dioxide to formic acid and carbon monoxide on metal electrodes. *ACS Catal.* 2017;7(7):4822–7.
104. Hatsukade T, Kuhl KP, Cave ER, Abram DN, Jaramillo TF. Insights into the electrocatalytic reduction of CO<sub>2</sub> on metallic silver surfaces. *Phys Chem Chem Phys.* 2014;16(27):13814–9.
105. Kim C, Jeon HS, Eom T, Jee MS, Kim H, Friend CM, Min BK, Hwang YJ. Achieving selective and efficient electrocatalytic activity for CO<sub>2</sub> reduction using immobilized silver nanoparticles. *J Am Chem Soc.* 2015;137(43):13844–50.
106. Zhu WL, Michalsky R, Metin O, Lv HF, Guo SJ, Wright CJ, Sun XL, Peterson AA, Sun SH. Monodisperse Au nanoparticles for selective electrocatalytic reduction of CO<sub>2</sub> to CO. *J Am Chem Soc.* 2013;135(45):16833–6.
107. Nursanto EB, Jeon HS, Kim C, Jee MS, Koh JH, Hwang YJ, Min BK. Gold catalyst reactivity for CO<sub>2</sub> electro-reduction: from nano particle to layer. *Catal Today.* 2016;260:107–11.
108. Verma S, Hamasaki Y, Kim C, Huang WX, Lu S, Jhong HRM, Gewirth AA, Fujigaya T, Nakashima N, Kenis PJA. Insights into the low overpotential electroreduction of CO<sub>2</sub> to CO on a supported gold catalyst in an alkaline flow electrolyzer. *ACS Energy Lett.* 2018;3(1):193–8.
109. Mistry H, Reske R, Zeng ZH, Zhao ZJ, Greeley J, Strasser P, Roldan Cuenya B. Exceptional size-dependent activity enhancement in the electroreduction of CO<sub>2</sub> over Au nanoparticles. *J Am Chem Soc.* 2014;136(47):16473–6.
110. Yoon Y, Hall AS, Surendranath Y. Tuning of silver catalyst mesostructure promotes selective carbon dioxide conversion into fuels. *Angew Chem Int Ed.* 2016;55(49):15282–6.
111. Hall AS, Yoon Y, Wuttig A, Surendranath Y. Mesostructure-induced selectivity in CO<sub>2</sub> reduction catalysis. *J Am Chem Soc.* 2015;137(47):14834–7.
112. Zhu WL, Zhang YJ, Zhang HY, Lv HF, Li Q, Michalsky R, Peterson AA, Sun SH. Active and selective conversion of CO<sub>2</sub> to CO on ultrathin Au nanowires. *J Am Chem Soc.* 2014;136(46):16132–5.
113. Liu M, Pang YJ, Zhang B, De Luna P, Voznyy O, Xu JX, Zheng XL, Dinh CT, Fan FJ, Cao CH, et al. Enhanced electrocatalytic CO<sub>2</sub> reduction via field-induced reagent concentration. *Nature.* 2016;537(7620):382.
114. Safaei TS, Mephram A, Zheng XL, Pang YJ, Dinh CT, Liu M, Sinton D, Kelley SO, Sargent EH. High-density nanosharp microstructures enable efficient CO<sub>2</sub> electroreduction. *Nano Lett.* 2016;16(11):7224–8.
115. Lee HE, Yang KD, Yoon SM, Ahn HY, Lee YY, Chang HJ, Jeong DH, Lee YS, Kim MY, Nam KT. Concave rhombic dodecahedral Au nanocatalyst with multiple high-index facets for CO<sub>2</sub> reduction. *ACS Nano.* 2015;9(8):8384–93.
116. Kim JH, Woo H, Choi JW, Jung HW, Kim YT. CO<sub>2</sub> electroreduction on Au/TiC enhanced activity due to metal-support interaction. *ACS Catal.* 2017;7(3):2101–6.
117. Won DH, Shin H, Koh J, Chung J, Lee HS, Kim H, Woo SI. Highly efficient, selective, and stable CO<sub>2</sub> electroreduction on a hexagonal Zn catalyst. *Angew Chem Int Ed.* 2016;55(32):9297–300.
118. Rosen J, Hutchings GS, Lu Q, Forest RV, Moore A, Jiao F. Electrodeposited Zn dendrites with enhanced CO selectivity for electrocatalytic CO<sub>2</sub> reduction. *ACS Catal.* 2015;5(8):4586–91.
119. Quan FJ, Zhong D, Song HC, Jia FL, Zhang LZ. A highly efficient zinc catalyst for selective electroreduction of carbon dioxide in aqueous NaCl solution. *J Mater Chem A.* 2015;3(32):16409–13.
120. Gao DF, Zhou H, Wang J, Miao S, Yang F, Wang GX, Wang JG, Bao XH. Size-dependent electrocatalytic reduction of CO<sub>2</sub> over Pd nanoparticles. *J Am Chem Soc.* 2015;137(13):4288–91.
121. Gao DF, Zhou H, Cai F, Wang JG, Wang GX, Bao XH. Pd-containing nanostructures for electrochemical CO<sub>2</sub> reduction reaction. *ACS Catal.* 2018;8(2):1510–9.
122. Cho M, Song JT, Back S, Jung Y, Oh J. The role of adsorbed CN and Cl on an Au electrode for electrochemical CO<sub>2</sub> reduction. *ACS Catal.* 2018;8(2):1178–85.
123. Jiang K, Kharel P, Peng YD, Gangishetty MK, Lin HYG, Stavitski E, Attenkofer K, Wang HT. Silver nanoparticles with surface-bonded oxygen for highly selective CO<sub>2</sub> reduction. *ACS Sustain Chem Eng.* 2017;5(10):8529–34.
124. Kim C, Eom T, Jee MS, Jung H, Kim H, Min BK, Hwang YJ. Insight into electrochemical CO<sub>2</sub> reduction on surface-molecule mediated Ag nanoparticles. *ACS Catal.* 2017;7(1):779–85.
125. Lee CW, Cho NH, Yang KD, Nam KT. Reaction mechanisms of the electrochemical conversion of carbon dioxide to formic acid on tin oxide electrodes. *ChemElectroChem.* 2017;4(9):2130–6.
126. Yoo JS, Christensen R, Vegge T, Norskov JK, Studt F. Theoretical insight into the trends that guide the electrochemical reduction of carbon dioxide to formic acid. *ChemSusChem.* 2016;9(4):358–63.
127. He JF, Johnson NJJ, Huang AX, Berlinguette CP. Electrocatalytic alloys for CO<sub>2</sub> reduction. *ChemSusChem.* 2018;11(1):48–57.
128. Chen YH, Kanan MW. Tin oxide dependence of the CO<sub>2</sub> reduction efficiency on tin electrodes and enhanced activity for tin/tin oxide thin-film catalysts. *J Am Chem Soc.* 2012;134(4):1986–9.
129. Zhang S, Kang P, Meyer TJ. Nanostructured tin catalysts for selective electrochemical reduction of carbon dioxide to formate. *J Am Chem Soc.* 2014;136(5):1734–7.
130. Gu J, Heroguel F, Luterbacher J, Hu XL. Densely packed, ultra small SnO nanoparticles for enhanced activity and selectivity in electrochemical CO<sub>2</sub> reduction. *Angew Chem Int Ed.* 2018;57(11):2943–7.
131. Kumar B, Atla V, Brian JP, Kumari S, Nguyen TQ, Sunkara M, Spurgeon JM. Reduced SnO<sub>2</sub> porous nanowires with a high density of grain boundaries as



- catalysts for efficient electrochemical CO<sub>2</sub>-into-HCOOH conversion. *Angew Chem Int Ed.* 2017;56(13):3645–9.
132. Li FW, Chen L, Knowles GP, MacFarlane DR, Zhang J. Hierarchical mesoporous SnO<sub>2</sub> nanosheets on carbon cloth: a robust and flexible electrocatalyst for CO<sub>2</sub> reduction with high efficiency and selectivity. *Angew Chem Int Ed.* 2017;56(2):505–9.
133. Won DH, Choi CH, Chung J, Chung MW, Kim EH, Woo SI. Rational design of a hierarchical tin dendrite electrode for efficient electrochemical reduction of CO<sub>2</sub>. *ChemSusChem.* 2015;8(18):3092–8.
134. Zheng XL, De Luna P, de Arquer FPG, Zhang B, Becknell N, Ross MB, Li YF, Banis MN, Li YZ, Liu M, et al. Sulfur-modulated tin sites enable highly selective electrochemical reduction of CO<sub>2</sub> to formate. *Joule.* 2017;1(4):794–805.
135. Han N, Wang Y, Yang H, Deng J, Wu JH, Li YF, Li YG. Ultrathin bismuth nanosheets from in situ topotactic transformation for selective electrocatalytic CO<sub>2</sub> reduction to formate. *Nat Commun.* 2018;9:1320.
136. Lee CH, Kanan MW. Controlling H<sup>+</sup> vs CO<sub>2</sub> reduction selectivity on Pb electrodes. *ACS Catal.* 2015;5(1):465–9.
137. Hara K, Kudo A, Sakata T. Electrochemical reduction of carbon-dioxide under high-pressure on various electrodes in an aqueous-electrolyte. *J Electroanal Chem.* 1995;391(1–2):141–7.
138. Melchionna M, Bracamonte MV, Giuliani A, Nasi L, Montini T, Tavagnacco C, Bonchio M, Fornasiero P, Prato M. Pd@TiO<sub>2</sub>/carbon nanohorn electrocatalysts: reversible CO<sub>2</sub> hydrogenation to formic acid. *Energy Environ Sci.* 2018;11(6):1571–80.
139. Min XQ, Kanan MW. Pd-catalyzed electrohydrogenation of carbon dioxide to formate: high mass activity at low overpotential and identification of the deactivation pathway. *J Am Chem Soc.* 2015;137(14):4701–8.
140. Kuhl KP, Cave ER, Abram DN, Jaramillo TF. New insights into the electrochemical reduction of carbon dioxide on metallic copper surfaces. *Energy Environ Sci.* 2012;5(5):7050–9.
141. Sandberg RB, Montoya JH, Chan K, Norskov JK. CO-CO coupling on Cu facets: coverage, strain and field effects. *Surf Sci.* 2016;654:56–62.
142. Montoya JH, Peterson AA, Norskov JK. Insights into CC coupling in CO<sub>2</sub> electroreduction on copper electrodes. *ChemCatChem.* 2013;5(3):737–42.
143. Garza AJ, Bell AT, Head-Gordon M. Mechanism of CO<sub>2</sub> reduction at copper surfaces: pathways to C-2 products. *ACS Catal.* 2018;8(2):1490–9.
144. Hori Y, Murata A, Takahashi R. Formation of hydrocarbons in the electrochemical reduction of carbon-dioxide at a copper electrode in aqueous-solution. *J Chem Soc Faraday Trans 1.* 1989;85:2309–26.
145. Peterson AA, Abild-Pedersen F, Studt F, Rossmeisl J, Norskov JK. How copper catalyzes the electroreduction of carbon dioxide into hydrocarbon fuels. *Energy Environ Sci.* 2010;3(9):1311–5.
146. Huang Y, Handoko AD, Hirunsit P, Yeo BS. Electrochemical reduction of CO<sub>2</sub> using copper single-crystal surfaces: effects of CO\* coverage on the selective formation of ethylene. *ACS Catal.* 2017;7(3):1749–56.
147. Schouten KJP, Kwon Y, van der Ham CJM, Qin Z, Koper MTM. A new mechanism for the selectivity to C-1 and C-2 species in the electrochemical reduction of carbon dioxide on copper electrodes. *Chem Sci.* 2011;2(10):1902–9.
148. Lum YW, Cheng T, Goddard WA, Ager JW. Electrochemical CO reduction builds solvent water into oxygenate products. *J Am Chem Soc.* 2018; 140(30):9337–40.
149. Kas R, Kortlever R, Yilmaz H, Koper MTM, Mul G. Manipulating the hydrocarbon selectivity of copper nanoparticles in CO<sub>2</sub> electroreduction by process conditions. *ChemElectroChem.* 2015;2(3):354–8.
150. Jiang K, Sandberg RB, Akey AJ, Liu XY, Bell DC, Norskov JK, Chan KR, Wang HT. Metal ion cycling of Cu foil for selective C-C coupling in electrochemical CO<sub>2</sub> reduction. *Nat Catal.* 2018;1(2):111–9.
151. Loidjice A, Lobaccaro P, Kamali EA, Thao T, Huang BH, Ager JW, Buonsanti R. Tailoring copper nanocrystals towards C-2 products in electrochemical CO<sub>2</sub> reduction. *Angew Chem Int Ed.* 2016;55(19):5789–92.
152. Roberts FS, Kuhl KP, Nilsson A. High selectivity for ethylene from carbon dioxide reduction over copper nanocube electrocatalysts. *Angew Chem Int Ed.* 2015;54(17):5179–82.
153. Wang ZN, Yang G, Zhang ZR, Jin MS, Yin YD. Selectivity on etching: creation of high-energy facets on copper nanocrystals for CO<sub>2</sub> electrochemical reduction. *ACS Nano.* 2016;10(4):4559–64.
154. Hori Y, Takahashi I, Koga O, Hoshi N. Selective formation of C2 compounds from electrochemical reduction of CO<sub>2</sub> at a series of copper single crystal electrodes. *J Phys Chem B.* 2002;106(1):15–7.
155. Sen S, Liu D, Palmore GTR. Electrochemical reduction of CO<sub>2</sub> at copper nanofoams. *ACS Catal.* 2014;4(9):3091–5.
156. Cao L, Raciti D, Li CY, Livi KJT, Rottmann PF, Hemker KJ, Mueller T, Wang C. Mechanistic insights for low-overpotential electroreduction of CO<sub>2</sub> to CO on copper nanowires. *ACS Catal.* 2017;7(12):8578–87.
157. Ma M, Djanashvili K, Smith WA. Controllable hydrocarbon formation from the electrochemical reduction of CO<sub>2</sub> over Cu nanowire arrays. *Angew Chem Int Ed.* 2016;55(23):6680–4.
158. Huang P, Ci SQ, Wang GX, Jia JC, Xu JW, Wen ZH. High-activity Cu nanowires electrocatalysts for CO<sub>2</sub> reduction. *J CO<sub>2</sub> UTIL.* 2017;20:27–33.
159. Raciti D, Livi KJ, Wang C. Highly dense Cu nanowires for low-overpotential CO<sub>2</sub> reduction. *Nano Lett.* 2015;15(10):6829–35.
160. Ma M, Djanashvili K, Smith WA. Selective electrochemical reduction of CO<sub>2</sub> to CO on CuO-derived Cu nanowires. *Phys Chem Chem Phys.* 2015;17(32):20861–7.
161. Hoang TTH, Ma SC, Gold JI, Kenis PJA, Gewirth AA. Nanoporous copper films by additive-controlled electrodeposition: CO<sub>2</sub> reduction catalysis. *ACS Catal.* 2017;7(5):3313–21.
162. Song H, Im M, Song JT, Lim JA, Kim BS, Kwon Y, Ryu S, Oh J. Effect of mass transfer and kinetics in ordered Cu-mesostructures for electrochemical CO<sub>2</sub> reduction. *Appl Catal B.* 2018;232:391–6.
163. Yang KD, Ko WR, Lee JH, Kim SJ, Lee H, Lee MH, Nam KT. Morphology-directed selective production of ethylene or ethane from CO<sub>2</sub> on a Cu mesopore electrode. *Angew Chem Int Ed.* 2017;56(3):796–800.
164. De Luna P, Quintero-Bermudez R, Dinh CT, Ross MB, Bushuyev OS, Todorovic P, Regier T, Kelley SO, Yang PD, Sargent EH. Catalyst electrodeposition controls morphology and oxidation state for selective carbon dioxide reduction. *Nat Catal.* 2018;1(2):103–10.
165. Rahaman M, Dutta A, Zanetti A, Broekmann P. Electrochemical reduction of CO<sub>2</sub> into multicarbon alcohols on activated Cu mesh catalysts: an identical location (IL) study. *ACS Catal.* 2017;7(11):7946–56.
166. Jeon HS, Kunze S, Scholten F, Roldan Cuenya B. Prism-shaped Cu nanocatalysts for electrochemical CO<sub>2</sub> reduction to ethylene. *ACS Catal.* 2018;8(1):531–5.
167. Chung J, Won DH, Koh J, Kim EH, Woo SI. Hierarchical Cu pillar electrodes for electrochemical CO<sub>2</sub> reduction to formic acid with low overpotential. *Phys Chem Chem Phys.* 2016;18(8):6252–8.
168. Ren D, Deng YL, Handoko AD, Chen CS, Malkhandi S, Yeo BS. Selective electrochemical reduction of carbon dioxide to ethylene and ethanol on copper(I) oxide catalysts. *ACS Catal.* 2015;5(5):2814–21.
169. Kas R, Kortlever R, Milbrat A, Koper MTM, Mul G, Baltrusaitis J. Electrochemical CO<sub>2</sub> reduction on Cu<sub>2</sub>O-derived copper nanoparticles: controlling the catalytic selectivity of hydrocarbons. *Phys Chem Chem Phys.* 2014;16(24):12194–201.
170. Lee SY, Jung H, Kim NK, Oh HS, Min BK, Hwang YJ. Mixed copper states in anodized Cu electrocatalyst for stable and selective ethylene production from CO<sub>2</sub> reduction. *J Am Chem Soc.* 2018;140(28):8681–9.
171. Dinh CT, Burdyny T, Kibria MG, Seifitokaldani A, Gabardo CM, de Arquer FPG, Kiani A, Edwards JP, De Luna P, Bushuyev OS, et al. CO<sub>2</sub> electroreduction to ethylene via hydroxide-mediated copper catalysis at an abrupt interface. *Science.* 2018;360(6390):783–7.
172. Pander JE, Ren D, Huang Y, Loo NWX, Hong SHL, Yeo BS. Understanding the heterogeneous electrocatalytic reduction of carbon dioxide on oxide-derived catalysts. *ChemElectroChem.* 2018;5(2):219–37.
173. Lee S, Kim D, Lee J. Electrocatalytic production of C3-C4 compounds by conversion of CO<sub>2</sub> on a chloride-induced bi-phasic Cu<sub>2</sub>O-Cu catalyst. *Angew Chem Int Ed.* 2015;54(49):14701–5.
174. Chen YH, Li CW, Kanan MW. Aqueous CO<sub>2</sub> reduction at very low overpotential on oxide-derived Au nanoparticles. *J Am Chem Soc.* 2012; 134(49):19969–72.
175. Ma M, Trzesniewski BJ, Xie J, Smith WA. Selective and efficient reduction of carbon dioxide to carbon monoxide on oxide-derived nanostructured silver electrocatalysts. *Angew Chem Int Ed.* 2016;55(33):9748–52.
176. Verdaguier-Casadevall A, Li CW, Johansson TP, Scott SB, McKeown JT, Kumar M, Stephens IEL, Kanan MW, Chorkendorff I. Probing the active surface sites for CO reduction on oxide-derived copper electrocatalysts. *J Am Chem Soc.* 2015;137(31):9808–11.
177. Feng XF, Jiang KL, Fan SS, Kanan MW. A direct grain-boundary-activity correlation for CO electroreduction on Cu nanoparticles. *ACS Cent Sci.* 2016;2(3):169–74.
178. Mariano RG, McKelvey K, White HS, Kanan MW. Selective increase in CO<sub>2</sub> electroreduction activity at grain-boundary surface terminations. *Science.* 2017;358(6367):1187–91.
179. Eilert A, Cavalca F, Roberts FS, Osterwalder J, Liu C, Favaro M, Crumlin EJ, Ogasawara H, Friebel D, Pettersson LGM, et al. Subsurface oxygen in oxide-

- derived copper electrocatalysts for carbon dioxide reduction. *J Phys Chem Lett.* 2017;8(1):285–90.
180. Favaro M, Xiao H, Cheng T, Goddard WA, Yano J, Crumlin EJ. Subsurface oxide plays a critical role in CO<sub>2</sub> activation by Cu (111) surfaces to form chemisorbed CO<sub>2</sub>, the first step in reduction of CO<sub>2</sub>. *Proc Natl Acad Sci U S A.* 2017;114(26):6706–11.
181. Lum YW, Ager JW. Stability of residual oxides in oxide-derived copper catalysts for electrochemical CO<sub>2</sub> reduction investigated with O-18 labeling. *Angew Chem Int Ed.* 2018;57(2):551–4.
182. Clark EL, Hahn C, Jaramillo TF, Bell AT. Electrochemical CO<sub>2</sub> reduction over compressively strained CuAg surface alloys with enhanced multi-carbon oxygenate selectivity. *J Am Chem Soc.* 2017;139(44):15848–57.
183. Kim D, Resasco J, Yu Y, Asiri AM, Yang PD. Synergistic geometric and electronic effects for electrochemical reduction of carbon dioxide using gold-copper bimetallic nanoparticles. *Nat Commun.* 2014;5:4948.
184. Kim D, Xie CL, Becknell N, Yu Y, Karamad M, Chan K, Crumlin EJ, Norskov JK, Yang PD. Electrochemical activation of CO<sub>2</sub> through atomic ordering transformations of AuCu nanoparticles. *J Am Chem Soc.* 2017;139(24):8329–36.
185. Ma S, Sadakiyo M, Heima M, Luo R, Haasch RT, Gold JI, Yamauchi M, Kenis PJA. Electroreduction of carbon dioxide to hydrocarbons using bimetallic Cu-Pd catalysts with different mixing patterns. *J Am Chem Soc.* 2017;139(1):47–50.
186. Hirunsit P, Soodsawang W, Limtrakul J. CO<sub>2</sub> electrochemical reduction to methane and methanol on copper-based alloys: theoretical insight. *J Phys Chem C.* 2015;119(15):8238–49.
187. Larrazabal GO, Martin AJ, Mitchell S, Hauert R, Perez-Ramirez J. Enhanced reduction of CO<sub>2</sub> to CO over Cu-In electrocatalysts: catalyst evolution is the key. *ACS Catal.* 2016;6(9):6265–74.
188. Sarfraz S, Garcia-Esparza AT, Jedidi A, Cavallo L, Takanabe K. Cu-Sn bimetallic catalyst for selective aqueous electroreduction of CO<sub>2</sub> to CO. *ACS Catal.* 2016;6(5):2842–51.
189. Kortlever R, Peters I, Koper S, Koper MTM. Electrochemical CO<sub>2</sub> reduction to formic acid at low overpotential and with high faradaic efficiency on carbon-supported bimetallic Pd-Pt nanoparticles. *ACS Catal.* 2015;5(7):3916–23.
190. Luc W, Collins C, Wang SW, Xin HL, He K, Kang YJ, Jiao F. Ag-Sn bimetallic catalyst with a core-shell structure for CO<sub>2</sub> reduction. *J Am Chem Soc.* 2017;139(5):1885–93.
191. Choi SY, Jeong SK, Kim HJ, Baek IH, Park KT. Electrochemical reduction of carbon dioxide to formate on tin-lead alloys. *ACS Sustain Chem Eng.* 2016;4(3):1311–8.
192. Bai XF, Chen W, Zhao CC, Li SG, Song YF, Ge RP, Wei W, Sun YH. Exclusive formation of formic acid from CO<sub>2</sub> electroreduction by a tunable Pd-Sn alloy. *Angew Chem Int Ed.* 2017;56(40):12219–23.
193. Hahn C, Abram DN, Hansen HA, Hatsukade T, Jackson A, Johnson NC, Hellstern TR, Kuhl KP, Cave ER, Feaster JT, et al. Synthesis of thin film AuPd alloys and their investigation for electrocatalytic CO<sub>2</sub> reduction. *J Mater Chem A.* 2015;3(40):20185–94.
194. Liu X, Dai LM. Carbon-based metal-free catalysts. *Nat Rev Mater.* 2016;1(11):16064.
195. Asefa T. Metal-free and noble metal-free heteroatom-doped nanostructured carbons as prospective sustainable electrocatalysts. *Acc Chem Res.* 2016;49(9):1873–83.
196. Duan XC, Xu JT, Wei ZX, Ma JM, Guo SJ, Wang SY, Liu HK, Dou SX. Metal-free carbon materials for CO<sub>2</sub> electrochemical reduction. *Adv Mater.* 2017;29(41):1701784.
197. Guo DH, Shibuya R, Akiba C, Saji S, Kondo T, Nakamura J. Active sites of nitrogen-doped carbon materials for oxygen reduction reaction clarified using model catalysts. *Science.* 2016;351(6271):361–5.
198. Liu S, Yang HB, Huang X, Liu LH, Cai WZ, Gao JJ, Li XN, Zhang T, Huang YQ, Liu B. Identifying active sites of nitrogen-doped carbon materials for the CO<sub>2</sub> reduction reaction. *Adv Funct Mater.* 2018;28(21):1800499.
199. Xu JY, Kan YH, Huang R, Zhang BS, Wang BL, Wu KH, Lin YM, Sun XY, Li QF, Centi G, et al. Revealing the origin of activity in nitrogen-doped nanocarbons towards electrocatalytic reduction of carbon dioxide. *ChemSusChem.* 2016;9(10):1085–9.
200. Wu JJ, Yadav RM, Liu MJ, Sharma PP, Tiwary CS, Ma LL, Zou XL, Zhou XD, Yakobson BI, Lou J, et al. Achieving highly efficient, selective, and stable CO<sub>2</sub> reduction on nitrogen-doped carbon nanotubes. *ACS Nano.* 2015;9(5):5364–71.
201. Sharma PP, Wu JJ, Yadav RM, Liu MJ, Wright CJ, Tiwary CS, Yakobson BI, Lou J, Ajayan PM, Zhou XD. Nitrogen-doped carbon nanotube arrays for high-efficiency electrochemical reduction of CO<sub>2</sub>: on the understanding of defects, defect density, and selectivity. *Angew Chem Int Ed.* 2015;54(46):13701–5.
202. Wu JJ, Liu MJ, Sharma PP, Yadav RM, Ma LL, Yang YC, Zou XL, Zhou XD, Vajtai R, Yakobson BI, et al. Incorporation of nitrogen defects for efficient reduction of CO<sub>2</sub> via two-electron pathway on three-dimensional graphene foam. *Nano Lett.* 2016;16(1):466–70.
203. Wu JJ, Ma SC, Sun J, Gold JI, Tiwary C, Kim B, Zhu LY, Chopra N, Odeh IN, Vajtai R, et al. A metal-free electrocatalyst for carbon dioxide reduction to multi-carbon hydrocarbons and oxygenates. *Nat Commun.* 2016;7:13869.
204. Liu YM, Chen S, Quan X, Yu HT. Efficient electrochemical reduction of carbon dioxide to acetate on nitrogen-doped nanodiamond. *J Am Chem Soc.* 2015;137(36):11631–6.
205. Li WL, Seredych M, Rodriguez-Castellon E, Bandoz TJ. Metal-free nanoporous carbon as a catalyst for electrochemical reduction of CO<sub>2</sub> to CO and CH<sub>4</sub>. *ChemSusChem.* 2016;9(6):606–16.
206. Sreekanth N, Nazrulla MA, Vineesh TV, Sailaja K, Phani KL. Metal-free boron-doped graphene for selective electroreduction of carbon dioxide to formic acid/formate. *Chem Commun.* 2015;51(89):16061–4.
207. Kim J, Kim HE, Lee H. Single-atom catalysts of precious metals for electrochemical reactions. *ChemSusChem.* 2018;11(1):104–13.
208. Yang S, Kim J, Tak YJ, Soon A, Lee H. Single-atom catalyst of platinum supported on titanium nitride for selective electrochemical reactions. *Angew Chem Int Ed.* 2016;55(6):2058–62.
209. Choi CH, Kim M, Kwon HC, Cho SJ, Yun S, Kim HT, Mayrhofer KJJ, Kim H, Choi M. Tuning selectivity of electrochemical reactions by atomically dispersed platinum catalyst. *Nat Commun.* 2016;7:10922.
210. Deng J, Li HB, Xiao JP, Tu YC, Deng DH, Yang HX, Tian HF, Li JQ, Ren PJ, Bao XH. Triggering the electrocatalytic hydrogen evolution activity of the inert two-dimensional MoS<sub>2</sub> surface via single-atom metal doping. *Energy Environ Sci.* 2015;8(5):1594–601.
211. Kim J, Roh CW, Sahoo SK, Yang S, Bae J, Han JW, Lee H. Highly durable platinum single-atom alloy catalyst for electrochemical reactions. *Adv Eng Mater.* 2018;8(1):1701476.
212. Yang HB, Hung SF, Liu S, Yuan KD, Miao S, Zhang LP, Huang X, Wang HY, Cai WZ, Chen R, et al. Atomically dispersed Ni(i) as the active site for electrochemical CO<sub>2</sub> reduction. *Nat Energy.* 2018;3(2):140–7.
213. Jiang K, Siahrostami S, Zheng TT, Hu YF, Hwang S, Stavitski E, Peng YD, Dynes J, Gangisetty M, Su D, et al. Isolated Ni single atoms in graphene nanosheets for high-performance CO<sub>2</sub> reduction. *Energy Environ Sci.* 2018;11(4):893–903.
214. Jiang K, Siahrostami S, Akey AJ, Li YB, Lu ZY, Lattimer J, Hu YF, Stokes C, Gangishetty M, Chen GX, et al. Transition-metal single atoms in a graphene shell as active centers for highly efficient artificial photosynthesis. *Chem.* 2017;3(6):950–60.
215. Wang YF, Chen Z, Han P, Du YH, Gu ZX, Xu X, Zheng GF. Single-atomic Cu with multiple oxygen vacancies on ceria for electrocatalytic CO<sub>2</sub> reduction to CH<sub>4</sub>. *ACS Catal.* 2018;8(8):7113–9.
216. Backs S, Jung YS. TiC- and TiN-supported single-atom catalysts for dramatic improvements in CO<sub>2</sub> electrochemical reduction to CH<sub>4</sub>. *ACS Energy Lett.* 2017;2(5):969–75.
217. Back S, Lim J, Kim NY, Kim YH, Jung Y. Single-atom catalysts for CO<sub>2</sub> electroreduction with significant activity and selectivity improvements. *Chem Sci.* 2017;8(2):1090–6.
218. Cheng MJ, Clark EL, Pham HH, Bell AT, Head-Gordon M. Quantum mechanical screening of single-atom bimetallic alloys for the selective reduction of CO<sub>2</sub> to C-1 hydrocarbons. *ACS Catal.* 2016;6(11):7769–77.
219. Varela AS, Kroschel M, Reier T, Strasser P. Controlling the selectivity of CO<sub>2</sub> electroreduction on copper: the effect of the electrolyte concentration and the importance of the local pH. *Catal Today.* 2016;260:8–13.
220. Resasco J, Chen LD, Clark E, Tsai C, Hahn C, Jaramillo TF, Chan K, Bell AT. Promoter effects of alkali metal cations on the electrochemical reduction of carbon dioxide. *J Am Chem Soc.* 2017;139(32):11277–87.
221. Singh MR, Kwon Y, Lum Y, Ager JW, Bell AT. Hydrolysis of electrolyte cations enhances the electrochemical reduction of CO<sub>2</sub> over Ag and Cu. *J Am Chem Soc.* 2016;138(39):13006–12.
222. Verma S, Lu X, Ma SC, Masel RI, Kenis PJA. The effect of electrolyte composition on the electroreduction of CO<sub>2</sub> to CO on Ag based gas diffusion electrodes. *Phys Chem Chem Phys.* 2016;18(10):7075–84.
223. Rosen BA, Salehi-Khojin A, Thorson MR, Zhu W, Whipple DT, Kenis PJA, Masel RI. Ionic liquid-mediated selective conversion of CO<sub>2</sub> to CO at low overpotentials. *Science.* 2011;334(6056):643–4.

224. Asadi M, Kim K, Liu C, Addepalli AV, Abbasi P, Yasaee P, Phillips P, Behranginia A, Cerrato JM, Haasch R, et al. Nanostructured transition metal dichalcogenide electrocatalysts for CO<sub>2</sub> reduction in ionic liquid. *Science*. 2016;353(6298):467–70.
225. Cole EB, Lakkaraju PS, Rampulla DM, Morris AJ, Abelev E, Bocarsly AB. Using a one-electron shuttle for the multielectron reduction of CO<sub>2</sub> to methanol: kinetic, mechanistic, and structural insights. *J Am Chem Soc*. 2010;132(33):11539–51.
226. Han ZJ, Kortlever R, Chen HY, Peters JC, Agapie T. CO<sub>2</sub> reduction selective for C<sub>2</sub> products on polycrystalline copper with N-substituted pyridinium additives. *ACS Cent Sci*. 2017;3(8):853–9.
227. Kim B, Hillman F, Ariyoshi M, Fujikawa S, Kenis PJA. Effects of composition of the micro porous layer and the substrate on performance in the electrochemical reduction of CO<sub>2</sub> to CO. *J Power Sources*. 2016;312:192–8.

**Ready to submit your research? Choose BMC and benefit from:**

- fast, convenient online submission
- thorough peer review by experienced researchers in your field
- rapid publication on acceptance
- support for research data, including large and complex data types
- gold Open Access which fosters wider collaboration and increased citations
- maximum visibility for your research: over 100M website views per year

**At BMC, research is always in progress.**

Learn more [biomedcentral.com/submissions](https://biomedcentral.com/submissions)

